GEOMETRIC MODELLING OF SHEET METAL STAMPINGS

By

© EDMUND WAI-KWOK CHU, B.Eng.

A Thesis

Submitted to the School of Graduate Studies

in Partial Fulfilment of the Requirements

for the Degree

Master of Engineering

McMaster University

December 1980

In the memory of my father without whom this thesis would never have come to its final form.

Faith is the assurance of things hoped for, the conviction of things not seen.

MASTER OF ENGINEERING (1980) McMASTER UNIVERSITY
(Metal Forming) Hamilton, Ontario

TITLE: Geometric Modelling of Sheet Metal Stampings

AUTHOR: Edmund Wai-Kwok Chu, B.Eng. (McMaster University)

SUPERVISOR: Dr. R. Sowerby

NUMBER OF PAGES: xiii, 115

ABSTRACT

A technique has been developed for the assessment of the magnitude and direction of the principal finite strains from measurements made on a deformed pair of lines. The analytical procedure leads to the establishment of a symmetric second order tensor which is not one of the classical large deformation tensor defined in many Continuum Mechanics texts, but is much simpler in form and readily applicable to the determination of natural strains in sheet metal forming operations.

Another aspect of this work has been an attempt to provide a new method (Geometric Modelling) for blank development and the investigation of possible strain distributions in forming sheet metal components. It is a computer technique simulating the traditional manual calculations performed by experienced tool designers.

The present work describes the formulation of the fundamental theory of the method and the basic geometric assumptions which are employed. Two particular examples have been considered; one is forming a sheet on a smoothly analytically defined surface and the other is forming the corner section of an automotive stamping.

The detailed analytical procedure is implemented in FORTRAN code. The analysis has been performed without access to advanced computer graphics. However; the results suggest that the basic approach is feasible and that future modelling using interactive computer graphics may well be attainable.

ACKNOWLEDGEMENTS

I wish to acknowledge the assistance, guidance and continual encouragement of my supervisor, Professor R. Sowerby.

The valuable stimulation of the present research, the extensive discussion and support provided by Professor J.L. Duncan throughout the course of this work is sincerely acknowledged.

Many thanks are also extended to Dr. M.P. Sklad, Professor G.A. Oravas, and my fellow students whose discussions and comments helped me with this work.

I extend my appreciation for the financial support granted by the Natural Sciences and Engineering Research Council of Canada and by the Ford Motor Company, Dearborn.

Finally, I wish to thank Nancy Sine of the Engineering Word Processing Centre, for her expert typing of the manuscript.

TABLE OF CONTENTS

TABLE OF CONTENTS (continued)

TABLE OF CONTENTS (continued)

LIST OF SYMBOLS

SYMBOL	DESCRIPTION	UNIT
E	Finite strain parameter	
ε	Total strain	
U	Component of displacement of a node in the x-direction	in.
V	Component of displacement of a node in the y-direction	in.
L_o	Original side length of a square	in.
OA, OB, OC	Initial side lengths of an element	in.
OA', OB', OC'	Final side lengths of a deformed element	in.
x, y, z	Local coordinate of an element	
X, Y, Z	Referential coordinates	
α	Angle of rotation of the co-rotational axes w.r.t. the deformed element	deg.
θ_I	Orientation of the principal axes	deg.

SUBSCRIPTS

I	I = 1, 2, 3 principal axes
x, y, z	Co-rotational axes
x', y', z'	Local coordinate axes
A, B, C	Nodal points of an element
I, J, K, L	Vertices of an element in 3D space
i, j, k, l	Vertices of an element in the plane surface

LIST OF FIGURES

LIST OF FIGURES (continued)

LIST OF FIGURES (continued)

LIST OF FIGURES (continued)

CHAPTER 1

INTRODUCTION

Blank development is the process of finding the size and shape for cutting the initial sheet or blank in order to make a given stamping. For simple shapes such as cylindrical cups and rectangular boxes, a number of geometric and semi-empirical relations can be found in sheet metal texts [1,2]. These permit manual calculation of suitable blanks. Many stamped parts have arbitrary rather than simple analytical shapes, hence other techniques must be employed. Geometric modelling is one of such techniques, which will be developed in this present work.

During the past decade investigators have studied numerical methods of modelling the entire sheet metal forming process in order to obtain a suitable blank shape. Some of these methods will be reviewed and applications to metal working process will also be presented in the next Chapter. Amongst those, the most popular approach is the finite element method in which the inputs are:

- the mechanical properties of the sheet;
- the geometry of the tooling;
- friction between the sheet and the tooling;
- an assumed initial blank configuration;
- other process data such as clamping pressure and

boundary conditions.

Using this approach, the sheet forming process is modelled incrementally. At each step, compatibility and equilibrium conditions are satisfied within narrow limits and the approximation is continued until the final shape is achieved or until some unsatisfactory conditions such as a failure strain is indicated. If this occurs, changes are made in the input conditions; for example, by changing the boundary conditions or the tool geometry or the blank shape; the modelling is then repeated until a satisfactory final result is obtained.

The above approach is capable of accurate modelling within one percent of error and much useful information has been obtained. However, extensive computation is required even for parts of simple geometry. At the present time, the technique is not suitable for an interactive computer-aided design system where the designer feeds a particular shape into a timesharing computer terminal and within a short time receives a solution satisfying the initial and final constraints he has imposed. Although future generations of computers may permit this computation to be executed within a reasonable time limit, it is unlikely that the computational efficiency required to solve a sheet metal problem using the method described can ever be improved drastically.

Traditionally, tool geometry has been determined by experience or by an experimental process called "TRYOUT" in which an initial blank is drawn through an assumed punch shape. If wrinkling occurs during the process then draw beads can be incorporated into the tooling in order to reduce the tendency of the material to draw-in. The process is then repeated many times until a final correct result is achieved. However, the technique tends to become very tedious when dealing with more complex geometry and requires skills on the part of the tool designer.

In light of these situations, the present work has been undertaken. It is the first step in an entirely different approach to computer-aided blank development, namely geometric modelling. This approach differs from finite element modelling, but the general techniques used in minimizing computer storage are common to both models. The work does not aim to provide, in the mathematical sense, a solution to the forming problem but rather it is a computer-aid for the tool designer in dealing with some traditional geometric problems. It is hoped that this study will provide a good starting point for subsequent analysis such that many of the procedures embodied in the techniques described previously can be eliminated. The author does not intend in any sense to propose an alternative or a modification of the existing methods. There are three particular features of the proposed method and these are summarized below:

(i) As already mentioned, other analytical methods are based on the specification of boundary conditions and material behaviour and involve finding a solution in terms of a stress or strain distribution. The designer then changes the input data until a satisfactory solution is achieved. In the new method, the approach is turned around and the designer specifies the most desirable end result of the forming process. This can be done essentially in geometrical terms. The method utilizes a computer technique for finding a suitable blank shape and a strain distribution which are geometrically compatible with the constraints imposed by the designer.

(ii) Forces, equilibrium and mechanical properties of the sheet are not accounted for and hence the resulting strain distribution is kinematically acceptable but not necessarily physically possible. Only geometric constraints are satisfied in the model.

(iii) The surface geometry of the component is described by flat triangular facets, the analysis deals only with these elements and the surface to which it must conform after the stamping operation is completed. It is not an incremental analysis.

The technique provides a more efficient way of utilizing the skill and experience of the designer, it does not aim to replace this by a "black box" computer system for sheet metal tool design which does not require an understanding of the process on the part of the user.

CHAPTER 2

APPLICATIONS OF NUMERICAL METHODS TO FORMING PROCESSES

2.1 INTRODUCTION

When dealing with numerical methods, it is important to realize what is necessary for, and what is required from, a final solution. If the requirement is an estimate of a load or pressure to carry out a forming operation, or if it is required to know how the load is affected by changing certain process parameters, a rigid-plastic analysis is often suitable. Slab or force balance methods [1, 2, 3, 4], upper bound and lower bound approaches [1, 4, 5, 6], slip line field (s.l.f.) analyses [4, 7] and finite element methods [1, 8, 9] are some of the solution procedures that have contributed in this regard. For a more detailed discussion see Ref. [21].

An elastic-plastic analysis is valuable for the determination of residual stresses and in problems where the elastic strain is of the same order as the plastic strain. It has also been widely applied in bifurcation studies. In these cases, it is necessary that the method of solution be capable of establishing a current distribution of stress as a function of the deformation history. The constitutive equation is usually formulated in terms of stress rates and strain rates. A more detailed discussion on these points are found in the articles by Lee et al. [1, 10], dealing with the development and applications of finite element methods to metal forming problems.

In this chapter some of the merits and limitations of certain numerical techniques which have been the most widely used in metal forming analyses are discussed. The theoretical fundamentals are to be found in many texts on plasticity and will not be given here. Instead an application of the methods is provided by solving a plane strain drawing problem. The solution procedures are given in detail in Appendix A.

2.2 NUMERICAL TECHNIQUES FOR SOLVING FORMING PROCESSES

2.2.1 The Slab Method

The elementary theory of the free body equilibrium approach i.e. the slab or force balance method was first developed by Siebel (1925) [1]. The technique relies on dividing the workpiece into a number of finite regions (strips, slabs, disks), the geometry of which depends on the nature of the problem. Each region is placed in force equilibrium. The method usually invokes the Tresca yield criterion and considers the material to be non-hardening (although allowance for work hardening can be made in an approximate manner by using a mean value of yield stress). It also permits an account to be taken of either Coulomb or constant shearing friction, it is to be noted that friction has often been treated as an adjustable parameter in order to provide the best correlation between theoretical predictions and experimental results.

Sachs [11] employed this technique to calculate the stress required to draw rod or wire through conical dies. Other investigators have sought improvements to Sach's equation by attempting to assess the influence of redundant work or work hardening, or both, on the drawing stress [12]. The application of this technique to analyse the direct drawing or extrusion of strip has been favourable [2, 6]. The method can also be used to estimate forging loads for quite complex forgings. The workpiece is divided into a number of modules, each of which is analysed separately and then recombined to provide estimate of the forging load. A recent review article by Altan and Nagpel [13] provides a comprehensive coverage of the current state of art on impression and closed die forging.

The slab method provides an unrealistic representation of the stress distribution within the deforming material because it is only obtained as a one-dimensional distribution. No account is taken of the inhomogeneity of the deformation, temperature and strain rate effects.

2.2.2 The Bounding Methods

Two extremum principles due to Hill [14] can be used to obtain "upper" and "lower" bounds for the loads to cause plastic flow. The practical applications of these principles has generally been restricted to rigid non-hardening solids deforming under plane strain conditions.

(a) Upper Bound Method

As the name implies, the technique provides an overestimate of the load(s) to effect plastic flow. The usual procedure is to divide the deformation region into a number of finite zones. The material moves as a rigid mass within each zone but is sheared as it crosses the boundary from one zone to another. The bounding lines are usually straight and a discontinuity in the tangential component of velocity occurs across each of these lines. From the pattern of discontinuity lines in the "physical plane" a corresponding velocity diagram (or hodograph) can be constructed. Certain velocity boundary conditions have to be satisfied, but no attempt is made to ensure that the material in each zone satisfies a yield criterion and there is no requirement that the individual zones are to be in equilibrium with each other. The rate of external working of the unknown traction (or load) is equated to the internal energy dissipated as material is sheared across each of the discontinuity lines. The method is usually adopted in the study of metal working problems since it provides an overestimate of the energy requirements to be delivered by a machine or press in order to execute the forming process.

(b) Lower Bound Method

Here again the material is divided up into a number of finite zones, similar to the discontinuity line pattern in the Upper Bound Method. However, in this case the emphasis is on establishing a statically admissible stress field (as opposed to a kinematically admissible velocity field). Each zone is placed in force equilibrium with its neighbour and it is stipulated that no zone has to exceed the yield criterion (the Tresca and Von Mises criteria take the same form under plane strain conditions). The unknown surface tractions are revealed through the equilibrium stress field.

The technique is often applied to structural analyses since it provides an underestimate of the load to cause plastic collapse.

It is to be noted that in general the Upper Bound and Lower Bound methods do not reveal a unique solution. However, adjustments can be made to the shape of the individual zones to reveal the lowest Upper Bound and the highest Lower Bound solution, for a basic zone pattern.

Upper Bound solutions far outweigh Lower Bound solutions in metalworking studies. In Refs. [1, 4, 6, 15, 16] there is to be found Upper Bound solutions for disc, ring and slab forging; wire and strip drawing; indenting; tube sinking and tube expansion; rolling of strip; direct, indirect, backward and hydrostatic extrusion; cutting and piercing. The readers' attention is drawn to the texts by Avitzur [6, 17], where emphasis is placed on Upper Bound Methods for other than plane strain deformation problems.

2.2.3 Slip Line Field Theory

Slip line field theory has been most widely applied in the study of plane strain deformation of rigid, non-hardening, solids. It contains features of both the Upper and Lower Bound methods, in that it permits a kinematically admissible velocity field along with a statically admissible stress field which satisfies the yielding condition within the deformation zone. It follows that the solutions obtained by the Upper and Lower Bound methods straddle (or bound from above and below) the slip line field solution.

The governing stress and velocity equations are hyperbolic and can be solved by the method of characteristics. It transpires that the characteristics for stress and velocity are identical and they lie in the direction of the maximum shear stress. Hence the deformation zone is covered by a network of orthogonal characteristics, and these are commonly referred to as the and slip lines.

Many similarities appear to exist (in fact these tend to be superficial) between a slip line field and upper bound solution. In both methods the physical plane is covered by a network of lines, from which a velocity diagram can be constructed. However, with the slip line field solution the network is orthogonal (i.e. the characteristics) and furthermore not all the slip lines have a discontinuity in the tangential component of velocity across them (this is always the case with the Upper Bound Method).

In statically determinate problems the usual procedure has been to build up a pattern of slip lines (based largely on experience) and to obtain the stress distribution within the deforming zone via the so called Hencky equations, i.e. the equilibrium equations reformulated along the characteristics. It is not always possible to proceed in this manner, in which case the slip line field and the hodograph have to be constructed simultaneously. In the past, this has led to laborious trial and error procedures (usually graphical) before an acceptable solution is obtained. A recent innovation, which obviates much of the labour with trial and error methods, is the matrix operational method due to Collins [18] and its subsequent development into a systematical computational procedure by Dewhurst and Collins [19].

As mentioned in the preceding section the Upper Bound Method has been applied to a variety of metal working operations. These same processes can also be studied using slip line field theory and in Refs. [1, 4, 7] a large number of examples are to be found.

One of the main criticisms levelled against slip line field theory is that it treats non-hardening solids only and ignores strain-hardening, strain-rate and temperature effects. Allowance can be made for strain hardening (see Ref. [20]) but the resulting stress equations along the characteristics lose their simplicity and recourse has to be made to numerical procedures to effect a solution. A similar situation arises when dealing with axi-symmetric problems involving rigid, non-hardening, solids*. The method of characteristics applied to plane stress problems is to be found in the recent text by Szczepinski [23].

---

* An interesting parallel can be drawn between the design of ideal (or streamlined) dies for both plane strain and axi-symmetric drawing (or extrusion) of a rigid, non-hardening, solid and the design of ideal gas nozzles [22], i.e., expansion nozzles, used in the supersonic flow of compressible gas. Both are constructed using the method of characteristics.

2.2.4 The Finite Element Method

The finite element method has been increasingly employed as an analytical tool in dealing with metal forming processes. However, its applications have largely been confined to problems with relatively simple geometry and to Problems with small plastic deformation. It has only been within the last decade or so that a proper formulation to account for large strain and/or large displacement problem has been embodied in a finite element code [10, 27].

The finite element approach involves the representation of a body or a structure by an assemblage of subdivisions called finite elements. These elements are interconnected at joints which are called nodes or nodal points. Simple displacement functions are chosen to approximate the distribution or variation of the actual displacement over each element. Other nodal quantities such as forces are usually considered. The principle of minimum potential is usually employed to obtain a set of equilibrium equations for each element; these equations, for the entire body, are then obtained by combining the equations for the individual elements in such a way that continuity of displacements or forces is preserved at the interconnecting nodes, the overall stiffness matrix for the whole body thus results. A lot of work has gone into investigating different types of elements and also the numerical procedures for solving the resulting matrix. However, this is outside the scope of the present survey, the interested reader is referred to the book by Zienkiewicz [8] for a more detailed discussion.

When dealing with metal working operations, the analysis is formulated in terms of either elastic-plastic solid (which is usually based on the elastic-plastic stress-strain matrix developed by Yamada et al. [24]) or rigid-plastic solid--the so-called matrix method developed by Lee and Kobayashi [25]. It uses the Lagrange multiplier in a variational formulation and linearization of nonlinear stiffness equations.

In hot forming processes the material is often treated as an incompressible non-Newtonian fluid, where the viscosity is related to the strain rate and possibly temperature and total strain. See the discussion in Ref. [26] which employs the finite element method to study the forming of superplastic alloys. The solution of large strain and/or large displacement problems are the subject of Refs. [10, 27], the reader is also referred to the article by Johnson and Sowerby [21] who review many metal forming processes solved by finite element methods.

2.3 DISCUSSION

Of the techniques discussed herein the finite element method is the most powerful (and also becoming the most widely employed) analytical tool for the study of bulk and sheet metal forming processes. It permits a more flexible material description, capable of accounting for elastic-plastic behaviour, temperature and strain rate effects. In addition, many more computer packages are becoming available which have the facility to deal with large strain and displacement problems. However, in metal forming processes the interfacial frictional conditions between tools and workpiece and certain boundary conditions are known imprecisely, and there is always some doubt about the appropriateness of any constitutive equation particularly when temperature and strain rates are involved. Consquently, even the most rigorous analytical procedure is controlled by the reliability of the input data. It is also to be noted that computer costs can become excessive and therefore the investigator must ask what he requires from a solution before embarking on more rigorous analytical techniques.

The bounding methods are relatively crude and in general deal with rate insensitive, rigid, perfectly plastic solids. However, solutions for the loads to effect plastic flow can be easily arrived at and in the first instance this may be the principal requirement of a designer of a press or forming machine.

Within the assumption of the plane strain deformation of a rigid non-hardening solid, slip line field theory is mathematically rigorous. It can provide insight into loads, stress distribution, material flow and the like for the two dimensional analog of many metal forming processes. The technique is usually restricted to steady state processes, otherwise incipient fields only are revealed. It has also been criticized because of the limited material description. However, if an attempt is made to incorporate strain hardening into the analysis the simplicity of the technique is lost and recourse has to be made to numerical procedures to effect a solution.

CHAPTER 3

EXPERIMENTAL STRAIN DETERMINATION

3.1 INTRODUCTION

This Chapter is concerned with finite deformation but it is not the intention to approach the topic in the traditional manner, as can be found in many texts on finite elasticity. The goal is the evaluation of the principal strains from measurements taken of a deformed grid of lines on a sheet metal pressing. With sheet metal components it is not unreasonable to ignore any variation in stress or strain through the thickness of the material and to treat the problem as one of plane stress*. In evaluating the principal strains some simplifying assumptions are made about the deformation mode, and hence the treatment is not completely general. However, as explained below these assumptions are implicit in the current practice of ascertaining the maximum strain level from measurements made on industrial pressings.

---

* Not necessarily a good assumption in the case of high contact stresses between tools/dies and workpiece, but these regions tend to be very localized and small in size compared to the overall size of the component.

3.1.1 Grid Measurements and Forming Limit Diagrams

The classical theory of plasticity is an incremental theory, in particular the increment of plastic strain in any deformation process is related to the current deviatoric stress state. In general the straining path followed by a general element in a plastically deforming body is not a proportional path. In other words, the principal axes of plastic strain (or strain increment) rotate with respect to the material element. Under these circumstances it is necessary to use an incremental approach and to sum (or integrate) in some manner each increment of plastic strain over the entire strain path, to arrive at the total (effective) strain. There are however, processes in which the straining path of an element is proportional, or nearly proportional. Thus in a pressing the situation could arise where it may not be unreasonable to assume that each element has attained its final configuration by a proportional straining path, although, in general, this path would not be the same for all elements.

While this assumption may be very much in error, it is the basis on which Forming Limit Diagrams (F.L.D.'s) are constructed. In this technique a grid of circles is photographically printed or electrochemically etched on a sheet metal blank. After deformation the circle has taken on a shape which is assumed to be an ellipse, and the major and minor diameter of an ellipse in the immediate vicinity of any fracture site on a pressing provides the principal (Limit) strains and a point on the Forming Limit Diagram. If the straining path was proportional then it is permissible to measure the final shape of the deformed grid circle to compute the strains since

$$\varepsilon_I = \int_0^{\varepsilon} d\varepsilon = \int_{\ell_o}^{\ell} \frac{d\ell}{\ell} = \ell n\left(\frac{\ell}{\ell_o} \right) \qquad (3.1)$$

In the above equation ℓ_o represents the initial diameter of the nth grid circle and ℓ is either the major or minor diameter of the deformed ellipse.

Under laboratory considerations it is possible to arrange that the straining process is proportional up to the point of fracture. Thus by altering the ratio of the principal strains a Forming Limit Diagram can be determined under these idealised conditions. Figure 3.1 provides a schematic representation of a FLD.

It has been reported from many sources that there can be a good correlation between an experimentally determined FLD and limit strains as measured on industrial pressings. However, this is not to say that such a correspondence would apply for all pressings, discrepancies have been noted and these usually attributed to non-proportional straining paths in that region of the pressing.

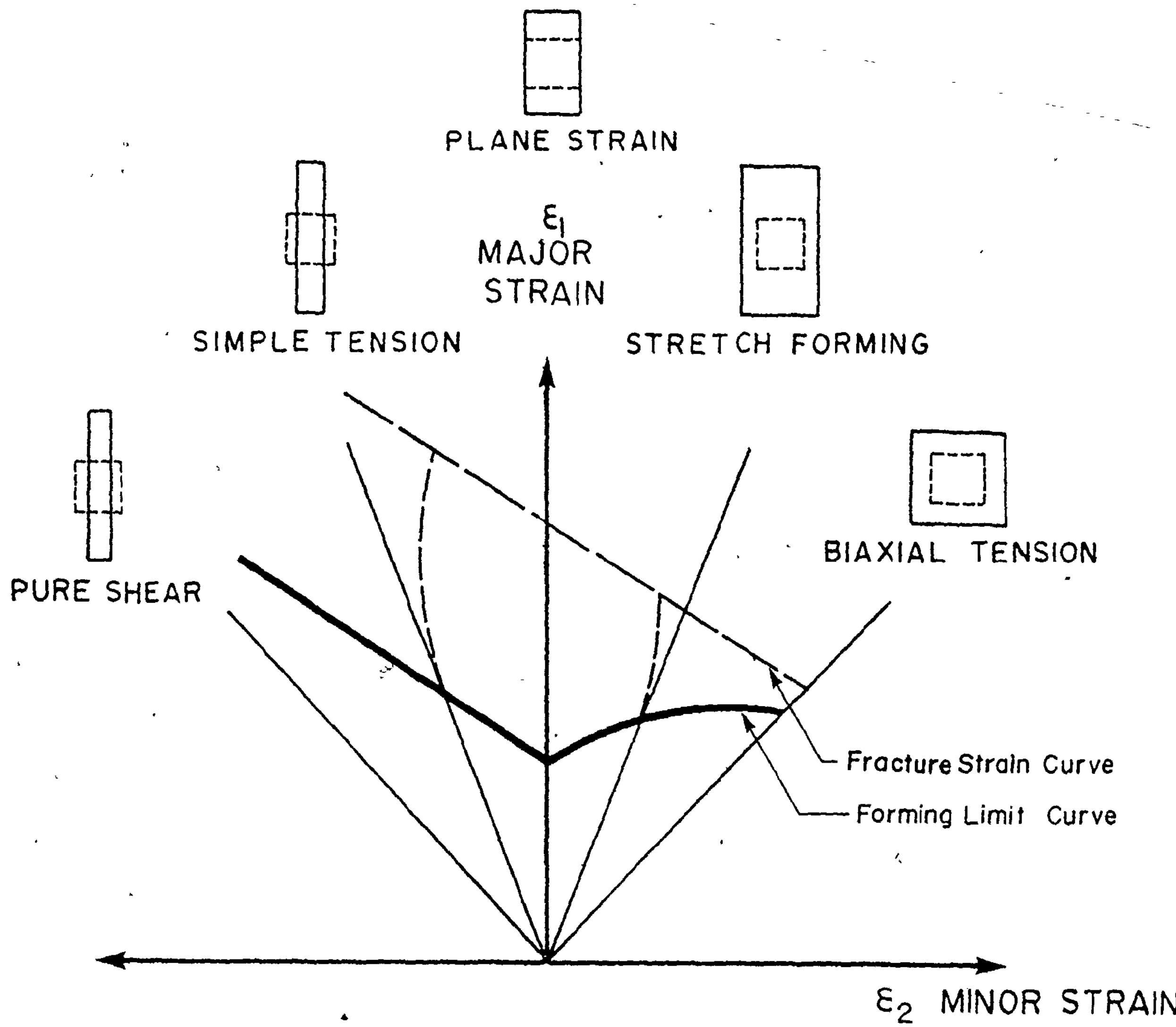

Figure 3.1 A schematic diagram showing the position of the forming limit curve and the fracture strain curve [28]

While the grid circle provides a convenient means of measuring strains, other types of grid patterns are employed. Common amongst these is a square or rectangular grid of lines, and Danckert and Wanhem [29] considered the problem of evaluating the strains from measurements made on a deformed square grid.

In the following sections some general comments are made about finite strain. Solution procedures are presented for evaluating the principal strains from measurements made on a deformed grid of lines. The simplifying assumption is that the straining path is linear throughout the deformation process.

3.2 FINITE ENGINEERING STRAIN

3.2.1 General Concepts

A body V_o as shown in Figure 3.2(a) is deformed to some configuration V. The deformation varies from point to point in the body and is considered to be large. However, in a small region b, surrounding some point P, it is assumed that:

(i) The deformation is monotonic and homogeneous within a sufficiently small volume;

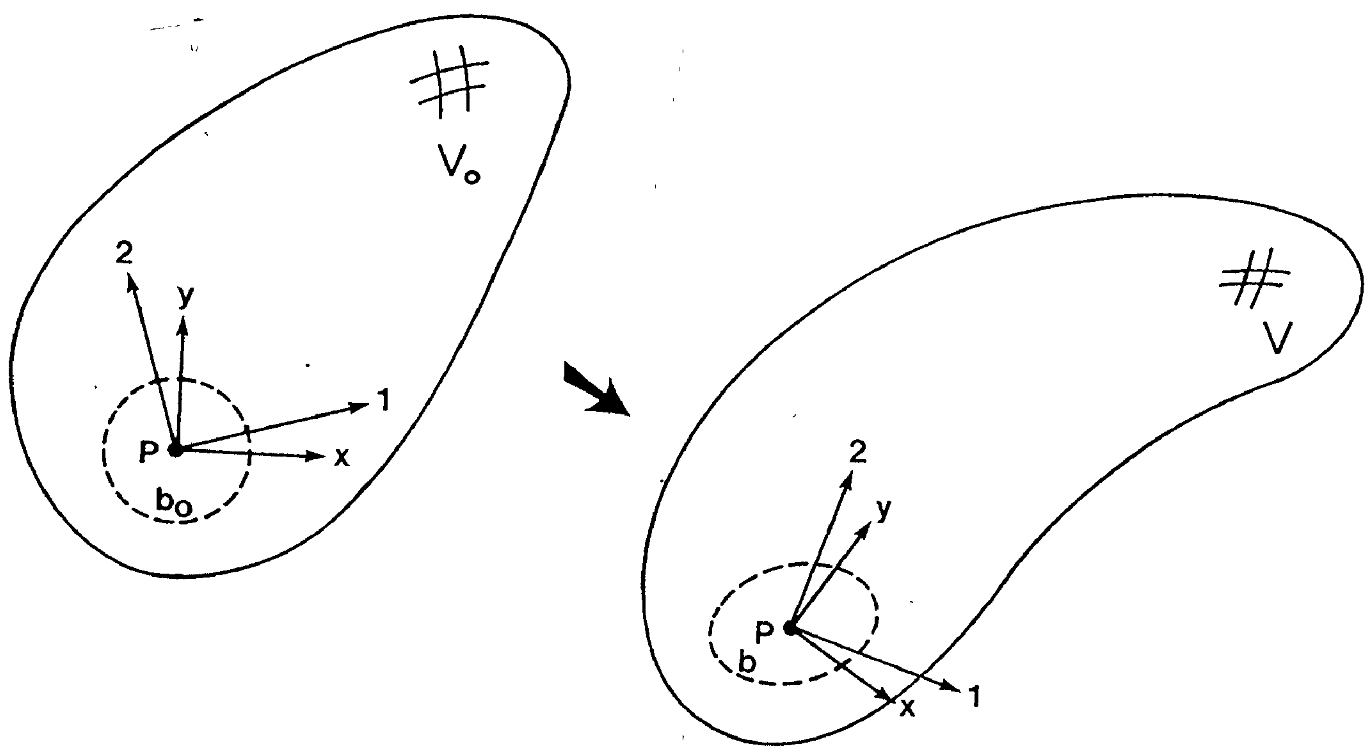

3.2(a) 3.2(b)

Figure 3.2 Diagrams illustrating the basic concepts
(a) Original undeformed body V_o
(b) Deformed body V

(ii) The principal axes I (1, 2 and 3) do not rotate relative to the material element so that points initially on such an axis move only along the axis;

(iii) The components of the total displacements of a point with respect to the principal axes can be described as a linear function of the initial coordinates X_I within the region b, i.e.,

$$U_I = E_I X_I \tag{3.2}$$

where E_I are the three instantaneous elongation coefficients.

The orientation of the principal axes together with the three elongation coefficients E_I completely define the final shape of the body, and the above conditions imply that an initial cube will deform into a parallelepiped. If the original cubic element in Figure 3.3 has side L then the current length of a side is

$$\ell_I = L_I + U_I = L_I\ (1 + E_I) \tag{3.3}$$

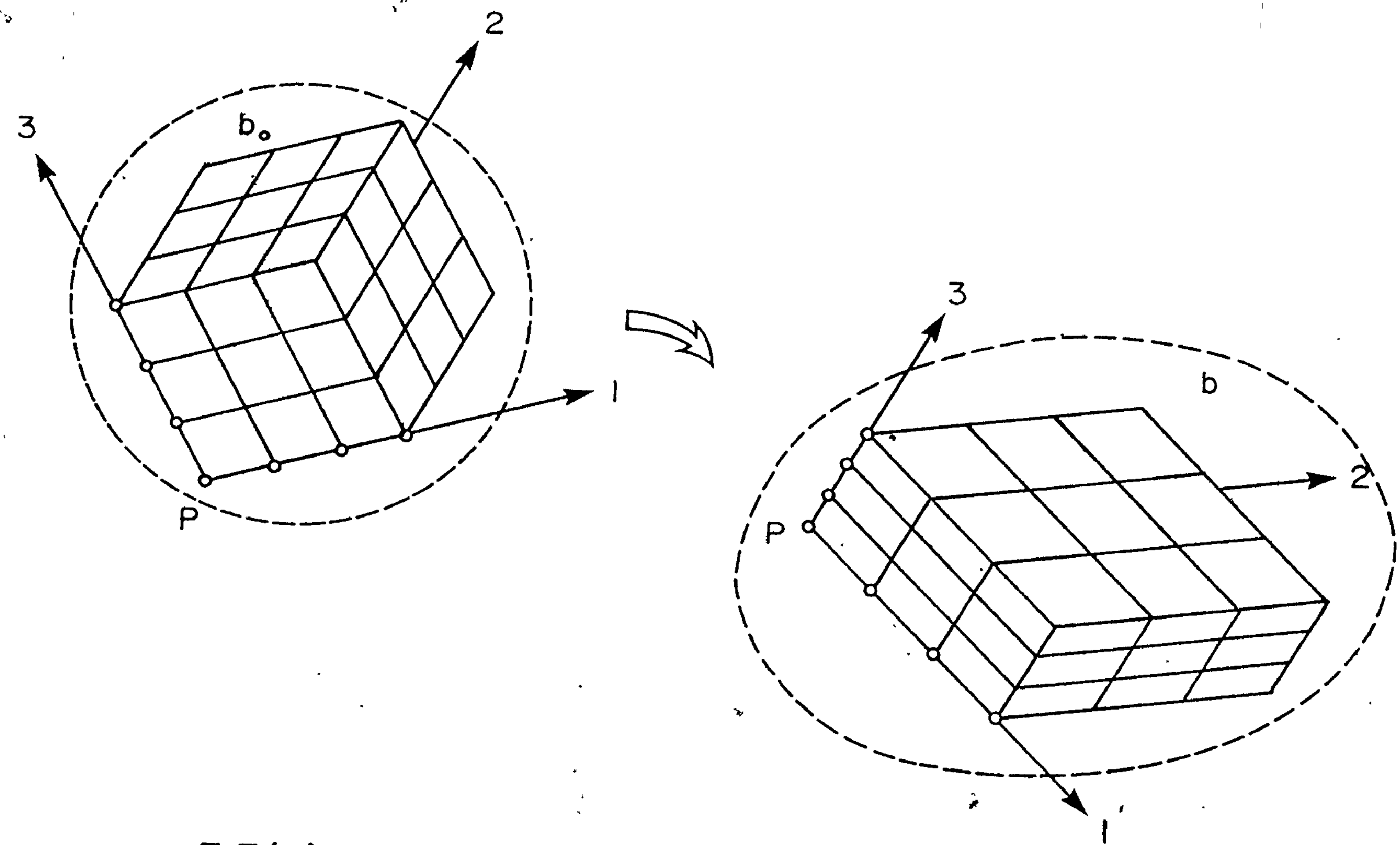

3.3(a) 3.3(b)

Figure 3.3 Deformation of a principal element within the region under consideration
(a) A cubic element in the unstrained state
(b) A cubic element in its deformed state

where the increment is

$$d\ell_I = L_I \, dE_I \tag{3.4}$$

It is required that ℓ_I changes smoothly and monotonically and that the total principal strains are defined by

$$\varepsilon_I = \int_0^{\ell} \frac{d\ell_I}{\ell_I} = \int_0^{E_I} \frac{dE_I}{1+E_I}$$

$$= \ell n(1 + E_I)$$

3.2.2 Elongation Coefficients

It is shown below that by identifying a new form of elongation coefficient, the principal strains and directions can be evaluated from measurements made on any pair of intersecting lines of arbitrary orientation to the principal axes. For illustrative purposes the initial grid is taken as square and the problem is assumed two dimensional, i.e., the third principal axis is taken perpendicular to the plane of the deformed grid. This later assumption would apply to most sheet metal formation problems.

As shown in Figure 3.4(a), a square grid of sides L_o within a region b_o in the undeformed state is considered. It is aligned with non-principal orthogonal axes x and y.

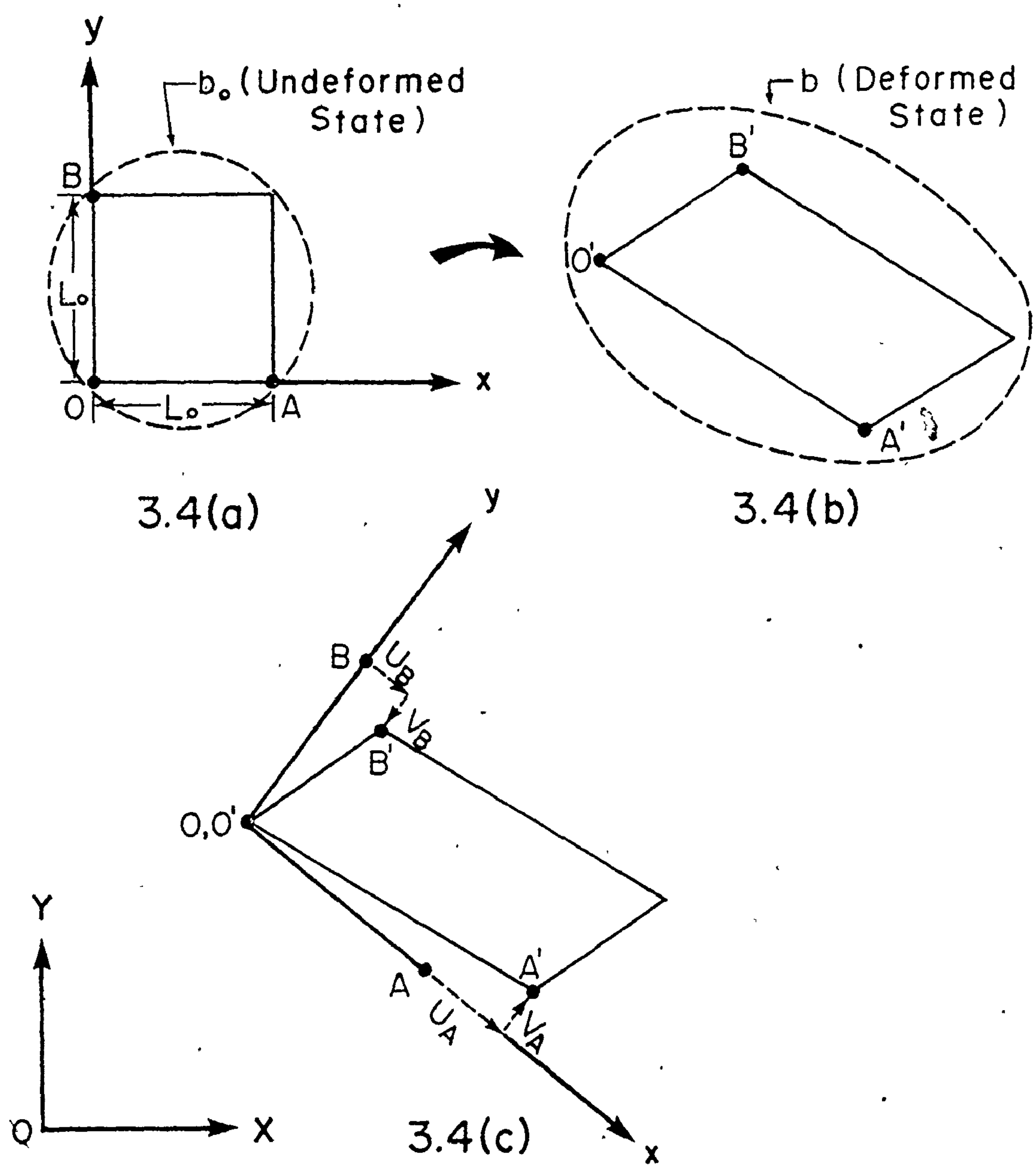

Figure 3.4 Deformation of a square grid
(a) Original unstrained element in a small region b_o
(b) Final deformed grid
(c) Components of the relative displacement with respect to the axes x-y

After deformation the grid is displaced to a new configuration involving translation and rotation, as shown in Figure 3.4(b).

The original x, y axes are now superimposed on the deformed grid such that

$$V_A = U_B \tag{3.5}$$

see Figure 3.4(c). Under a homogeneous deformation mode the material does deform such that (3.5) is satisfied. Note that this does not imply that the x and y axes are <u>equally inclined</u> to OA' and OB'.

In terms of the configuration of Figure 3.4(c), the elongation coefficients, or finite strain parameters [30, 31], are defined by:

$$\begin{aligned} E_{xx} &= U_A/L_o \\ E_{xy} &= V_A/L_o \\ E_{yx} &= U_B/L_o \\ E_{yy} &= V_B/L_o \end{aligned} \tag{3.6}$$

By virtue of (3.5)

$$E_{xy} = E_{yx}. \tag{3.7}$$

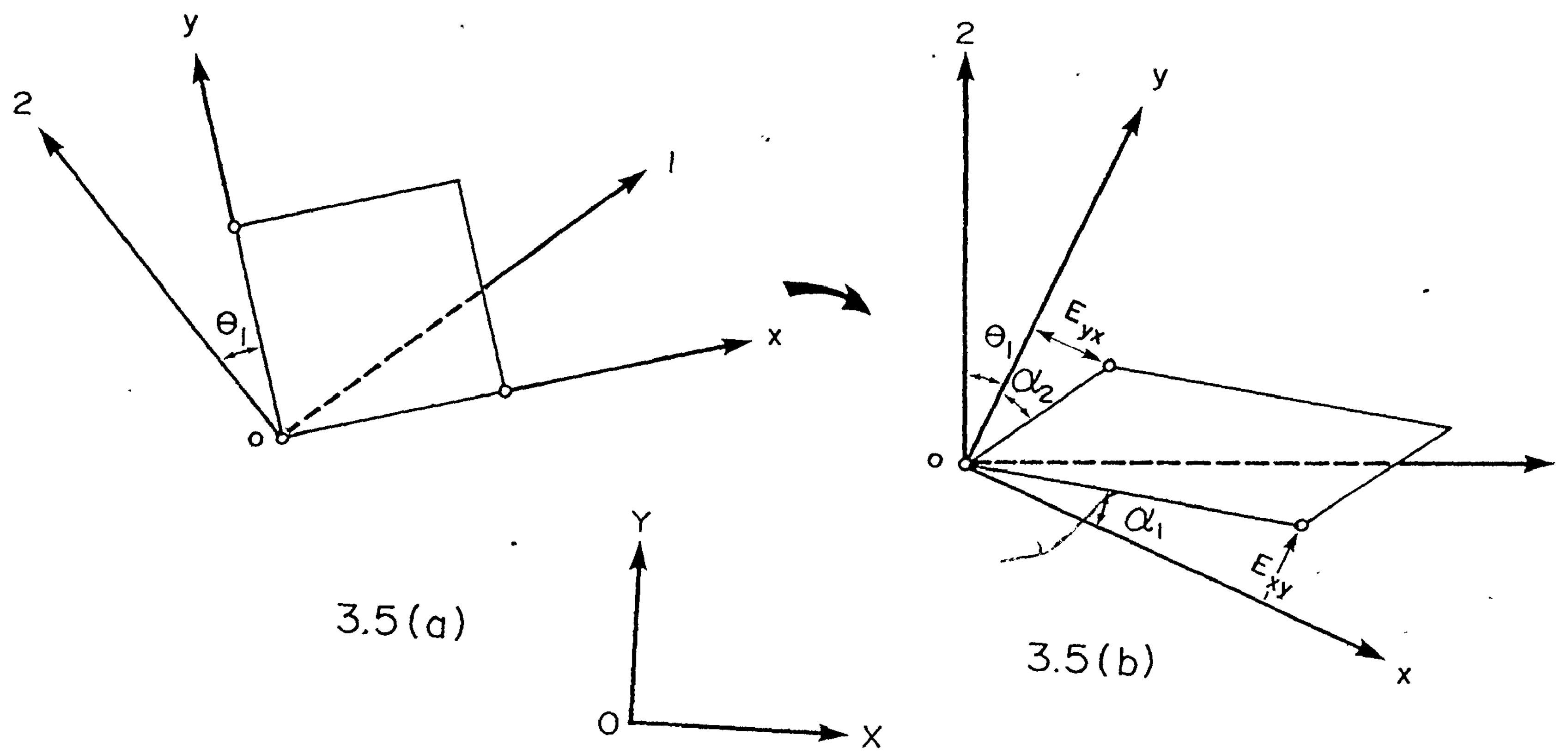

Figure 3.5 Two dimensional deformation of a square grid
(a) Initial square element
(b) Element is deformed into a parallelogram

It is the above property which permits the principal axes to be identified and reconstructed in the deformed state. This is illustrated in Figure 3.5 in which the z-axis coincides with the third principal direction.

3.2.3 Transformation of Finite Strain Parameters

For the two dimensional problem it is demonstrated in Appendix B how the finite strain parameters can be transformed from one set of orthogonal axes to another. The resulting expressions are

$$E_{x'x'} = \frac{E_{xx} + E_{yy}}{2} + \frac{E_{xx} - E_{yy}}{2} \cos 2\theta + E_{xy} \sin 2\theta$$

$$E_{x'y'} = - \frac{E_{xx} - E_{yy}}{2} \sin 2\theta + E_{xy} \cos 2\theta \qquad (3.8)$$

which are the transformation equations for any symmetric second order tensor. It follows that there exist principal values for the finite strain parameters (i.e. when $E_{x'y'}$ = 0) and for the two dimensional problem the transformation relationships are embodied in a Mohr's circle representation. This is discussed at greater length in Appendix B. In the usual manner the expression for the principal parameters is

$$E_{1,2} = \frac{E_{xx} + E_{yy}}{2} \pm \sqrt{\left(\frac{E_{xx} - E_{yy}}{2}\right)^2 + E_{xy}^2} \qquad (3.9)$$

and their orientation is given by

$$\tan 2\theta_1 = \frac{2E_{xy}}{E_{xx} - E_{yy}} \qquad (3.10)$$

The principal natural strains are

$$\varepsilon_{1,2} = \ln(1 + E_{1,2}) \qquad (3.11)$$

and the maximum value for E_{xy} is

$$(E_{xy})_{max} = \frac{E_1 - E_2}{2} \qquad (3.12)$$

For the three dimensional problem it follows in the usual manner [2] that the principal values are given by

$$\det \begin{vmatrix} E_{xx} - E_I & E_{xy} & E_{xz} \\ E_{yx} & E_{yy} - E_I & E_{yz} \\ E_{zx} & E_{zy} & E_{zz} - E_I \end{vmatrix} = 0 \qquad (3.13)$$

3.3 FINITE DEFORMATION OF OTHER PLANAR ELEMENTS

In this section the preceding analysis is extended to cover the deformations of both a rectangular grid and a quadrilateral element. A more detailed derivation can be found in Appendix C.

3.3.1 Deformation of a Rectangular Grid

The assumptions made in the preceding section regarding the deformation mode still hold but the displacements must now be related to the ratio of the original side lengths of the element, see Figure 3.6

$$\text{i.e.} \quad \frac{U_B}{V_A} = \frac{OB}{OA}$$

The strain parameters can be defined as:

$$\begin{aligned}
E_{xx} &= \frac{OA'}{OA}\cos\alpha - 1 \\
E_{xy} &= \frac{OA'}{OA}\sin\alpha \\
E_{yx} &= -\frac{OB'}{OB}\cos(\theta' - \alpha) \\
E_{yy} &= \frac{OB'}{OB}\sin(\theta' - \alpha) - 1
\end{aligned} \tag{3.15}$$

where θ' is the angle subtended by the deformed length OA' and OB', and

$$\alpha = \tan^{-1}\left(\frac{-OA \cdot OB' \cdot \cos\theta'}{OA' \cdot OB + OA \cdot OB' \cdot \sin\theta'}\right) \tag{3.16}$$

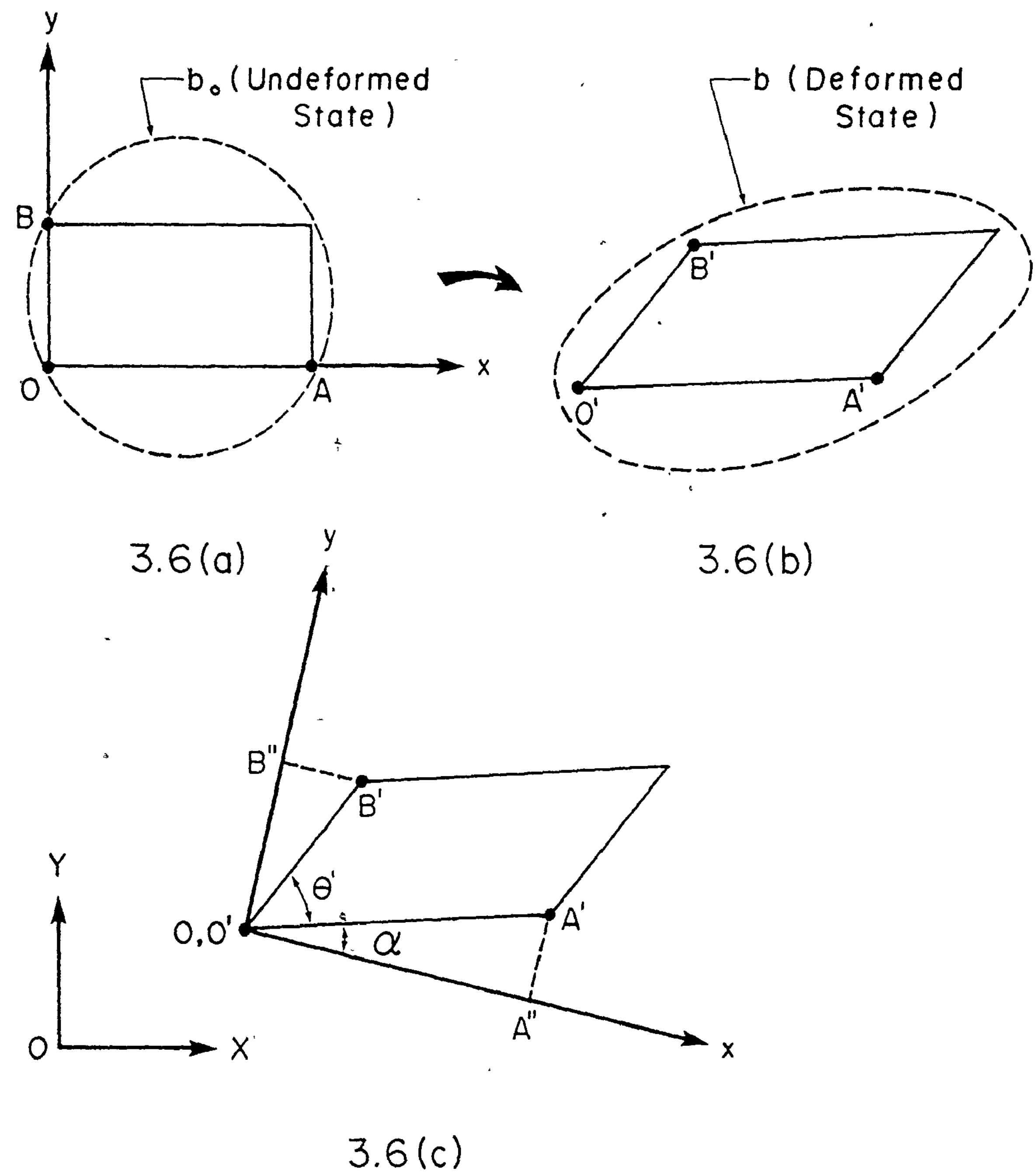

Figure 3.6 Deformation of a rectangular element
(a) Initial unstrained element within a small region b_o
(b) Deformed configuration of the element in (a)
(c) Deformed element together with the reconstructed axes

Again equation (3.14) leads to symmetric shear components i.e.

$$E_{xy} = E_{yx} \tag{3.17}$$

3.3.2 Deformation of a Parallelogram

A more detailed derivation is given in Appendix C, but a few comments can be made here.

Imagine that OB is part of a fictitious rectangular element as shown in Figure 3.7 such that a simple proportional deformation exists. This is the condition which allows the deformed configuration of the fictitious element to be determined. The finite strain parameters are given by:

$$\begin{aligned}
E_{xx} &= \frac{OA'}{OA}\cos\alpha - 1 \\
E_{xy} &= \frac{OA'}{OA}\sin\alpha \\
E_{yx} &= -\frac{OC'}{OC}\cos(\theta_1' - \alpha) \\
E_{yy} &= \frac{OC'}{OC}\sin(\theta_1' - \alpha) - 1
\end{aligned} \tag{3.18}$$

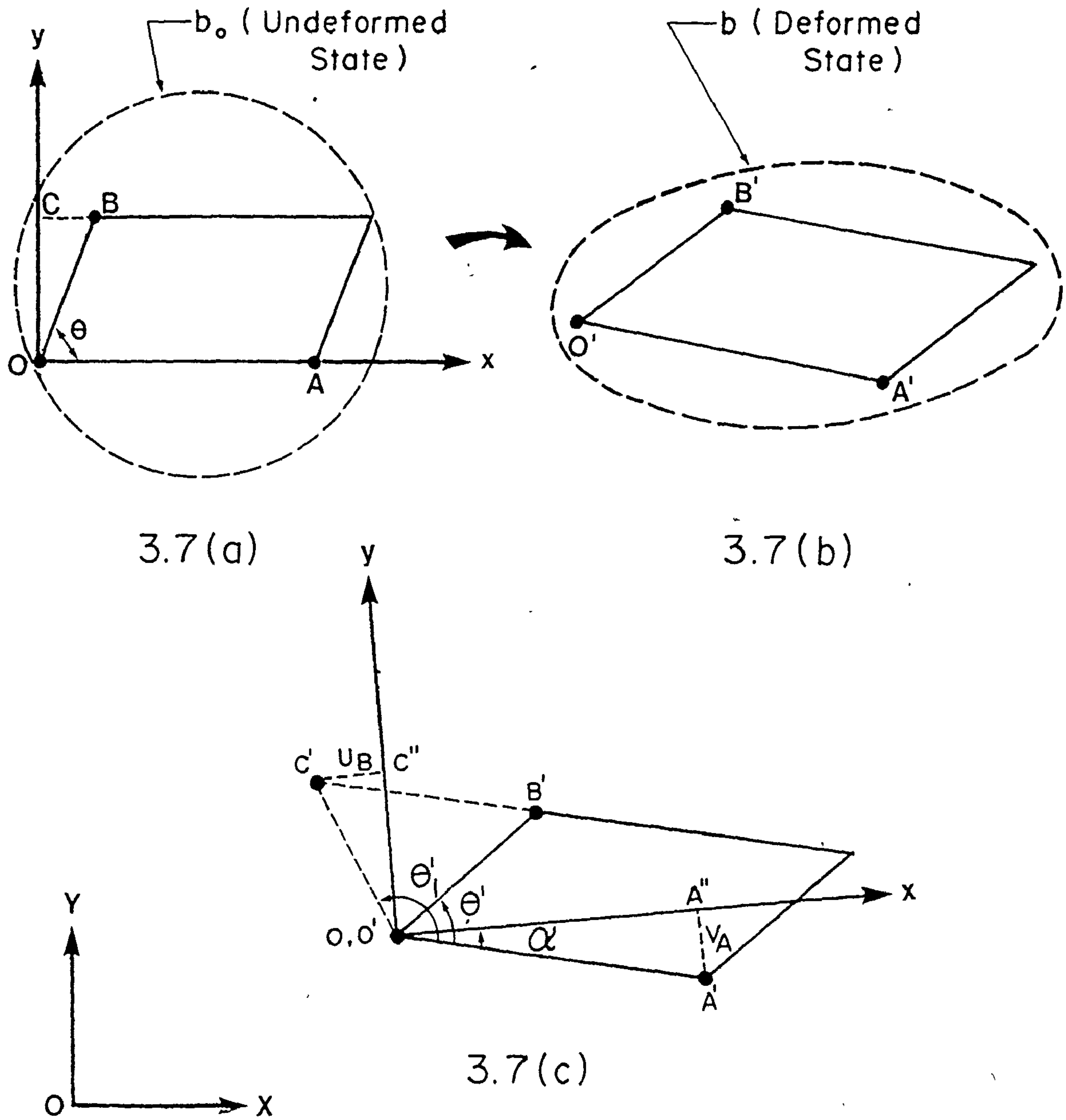

Figure 3.7 Deformation of a parallelogram
(a) Initial undeformed element
(b) Deformed state of the element
(c) Local coordinate axes of the element is reconstructed after deformation

where

$$\theta_1' = \tan^{-1}\left(\frac{OA \cdot OB' \cdot \sin\theta'}{OA \cdot OB' \cdot \cos\theta' - OA' \cdot OB \cdot \cos\theta}\right) \qquad (3.19)$$

θ is the original angle between sides OA and OB;

θ' is the deformed angle substained by sides OA' and OB';

$$\alpha = \tan^{-1}\left(\frac{-OA \cdot OC' \cdot \cos\theta_1'}{OA' \cdot OC + OA \cdot OC' \cdot \sin\theta_1'}\right) \qquad (3.20)$$

$$OC = OB \cdot \sin\theta$$

$$OC' = \frac{OB' \cdot \sin\theta'}{\sin\theta_1'}$$

The finite strain parameters developed in these two sections follow exactly the same transformation rules described previously.

3.4 DISCUSSION

The present Chapter has illustrated how the magnitude and direction of the principal strains can be determined from measurements made on a deformed pair of lines. The application to the assessment of strains on a sheet metal component is obvious. It is emphasized that the analysis is applicable strictly to a homogeneous deformation mode where the principal axes do not rotate with respect to the

-material element. However, the deformed configuration could be predicted by the present analysis if the state was reached by a discrete number of finite deformation steps i.e., strain in one particular homogeneous mode, followed by another and so on.

The reader may have a tendency to draw a comparison between the <u>finite</u> strain components E_{xx}, E_{xy}, etc. and the components defined for infinitesimal strains. However, the strain tensor defined here is truly a large strain (symmetric) tensor. It is not one of the classical finite strain tensors described in many texts on Continuum Mechanics. It is much simpler in form but can be shown to yield exactly the same values for principal strains [32].

CHAPTER 4

GEOMETRIC MODELLING

4.1 INTRODUCTION

A sheet metal pressing is usually produced by a combination of drawing and stretching. Having decided upon the basic form of the tooling/dies and the like, there usually results a series of press trials which decide the level of clamping (through draw rings) and the location of draw beads in order to produce a successful pressing. It will be appreciated that there is a complicated interplay of die geometry, lubrication conditions and the properties of the sheet material which governs the amount of effective clamping, i.e. the clamping has to be sufficient to offer resistance to the material and so prevent wrinkling or buckling, but at the same time allowing the material to "draw-in". If the material is over-restrained the material will not draw-in and all the deformation will take place by stretching; only very shallow parts could be formed by this technique. Although it is customary to use an initial sheet metal blank of simple geometric shapes such as rectangular or circular, this is usually not the optimum shape. The blank shape can promote or inhibit the inward flow of material in certain parts of the flange, and the amount of scrap which arises in the trim operation can be minimized with a correctly designed blank shape.

Traditionally the design of dies for sheet metal forming operations has relied more on technical expertise than detailed analysis. Quite often the designer envisages the die to be comprised of modules of simple geometric shapes, and significant dimensions are regarded as contour (line) lengths across different sections of the die. These contour lengths are used to interpret the size of the initial blank. Although the design methods appear crude it will be recognized that the tooling can be (and often is) very complex, and a successful pressing indicates the skill of the designer.

Finite difference and finite element procedures (particularly the latter) are being increasingly employed as analytical tools in the study of sheet metal forming problems. In such studies it is usual to consider that the basic shape of the tooling is known at the outset, along with the frictional conditions, material properties and boundary conditions. Given this information, the numerical procedure attempts to assess whether the sheet metal can be formed into the part without the occurrence of wrinkling, a fracture of the material - these two failure conditions are also regarded as known a priori. It will be appreciated that a lot of information is assumed known at the outset, and it is a moot point as to how well the assumptions correspond to the actual conditions. If, in the course of the computations the material is deemed to have failed before the component is fully formed, the only recourse is to alter one or more of the input conditions and repeat the calculation. At this time the only reported solutions using the finite element technique are for very simple axi-symmetric shapes. It can be anticipated that this numerical procedure will be applied to more complex shapes, provided that the computational costs can be kept within reasonable limits. A more interactive system(s) can also be envisaged where the critical regions of a pressing can be displayed on a screen as the deformation proceeds, thus aiding in assessing adjustments which may have to be made to the geometry of the tooling, the boundary conditions and the like.

In the present work results are presented of a preliminary investigation into a new approach for assessing the shape of a blank for a sheet metal pressing. The technique is one of geometric modelling and is intended as a computer aid for the experienced tool designer. No attempt is made to satisfy force equilibrium at point to point within the material, in fact the mechanical properties of the sheet material are not even considered.

4.2 GEOMETRIC OBJECTIVES IN SHEET FORMING

Geometric modelling allows the designer to specify the deformation mode he would like to achieve. The modelling then predicts a strain distribution for the sheet metal which would satisfy this objective geometrically. In principle this leaves the designer with a great deal of flexibility, however, in the initial stages of this work attention is restricted to one particular type of deformation mode.

Stamping operations consist of transforming the local elements of a flat sheet usually into a non-developable shape.* In practice this shape is achieved by a combination of two deformation processes - drawing and stretching. Drawing is a process of plastic shear in the plane of the sheet in which the principal strains are equal and opposite and distortion occurs without change of thickness, as shown in Figure 4.1(a). Stretching implies extension in both principal directions and this is obviously accompanied by thinning, as shown in Figure 4.1(b). It is assumed that each element in the sheet reaches its final state by a linear path. In some instances, this is not true and such stampings must be analyzed differently; in many cases, the

---

* A "developable" surface is one onto which a plane sheet can be applied without distortion and purely by bending or curving.

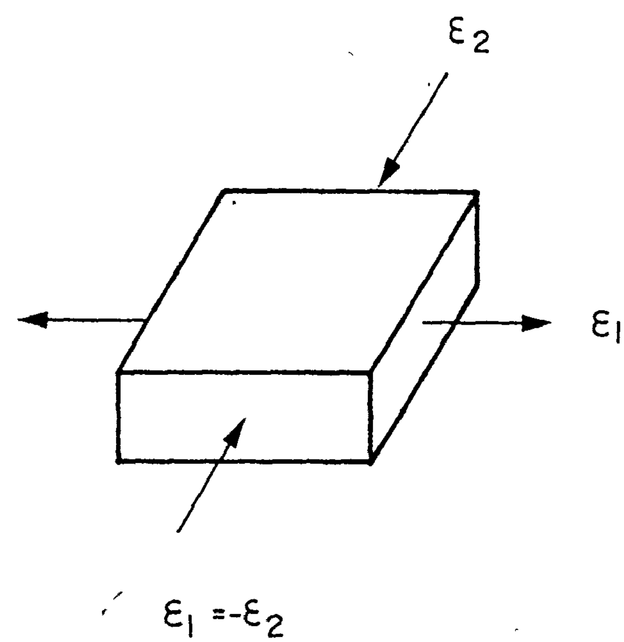

4.1(a)

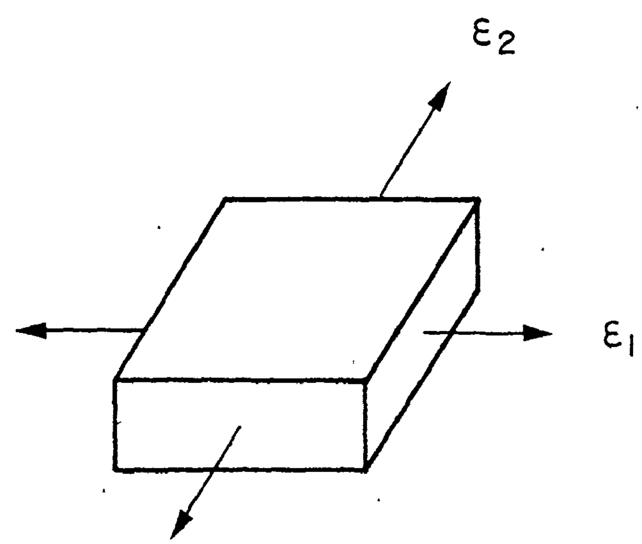

4.1(b)

Figure 4.1 Diagrams showing two common types of sheet metal forming processes.
(a) Drawing process
(b) Stretching process

assumption is appropriate. It has become customary to indicate sheet metal forming processes in terms of the forming limit diagram, as shown in Figure 4.2(a). In this diagram proportional straining of any element can be represented by a straight line radiating from the origin, as seen in Figure 4.2(b); biaxial stretching is represented by the right-hand diagonal while pure drawing by the left-hand diagonal. It is also found that for any one material, the onset of localized necking can be described by a forming limit curve as shown. This curve was first proposed by Keeler [34], but its origins lie in the work of Keeler and Backofen [35]. It is strongly dependent on the ratio of major and minor strains, but less dependent on other process variables.

Many materials with a low inherent ductility may fail suddenly before necking occurs and attempts have been made to describe this by means of a fracture map which is also shown in Figure 4.2(a). A third mode of failure is that of wrinkling but this appears to have received less attention, nevertheless it is not difficult to envisage that a wrinkling limit may exist, see reference [36].

An examination of the schematic diagram of Figure 4.2(a) indicates that the pure drawing is one of the deformation modes which is the least likely to be terminated

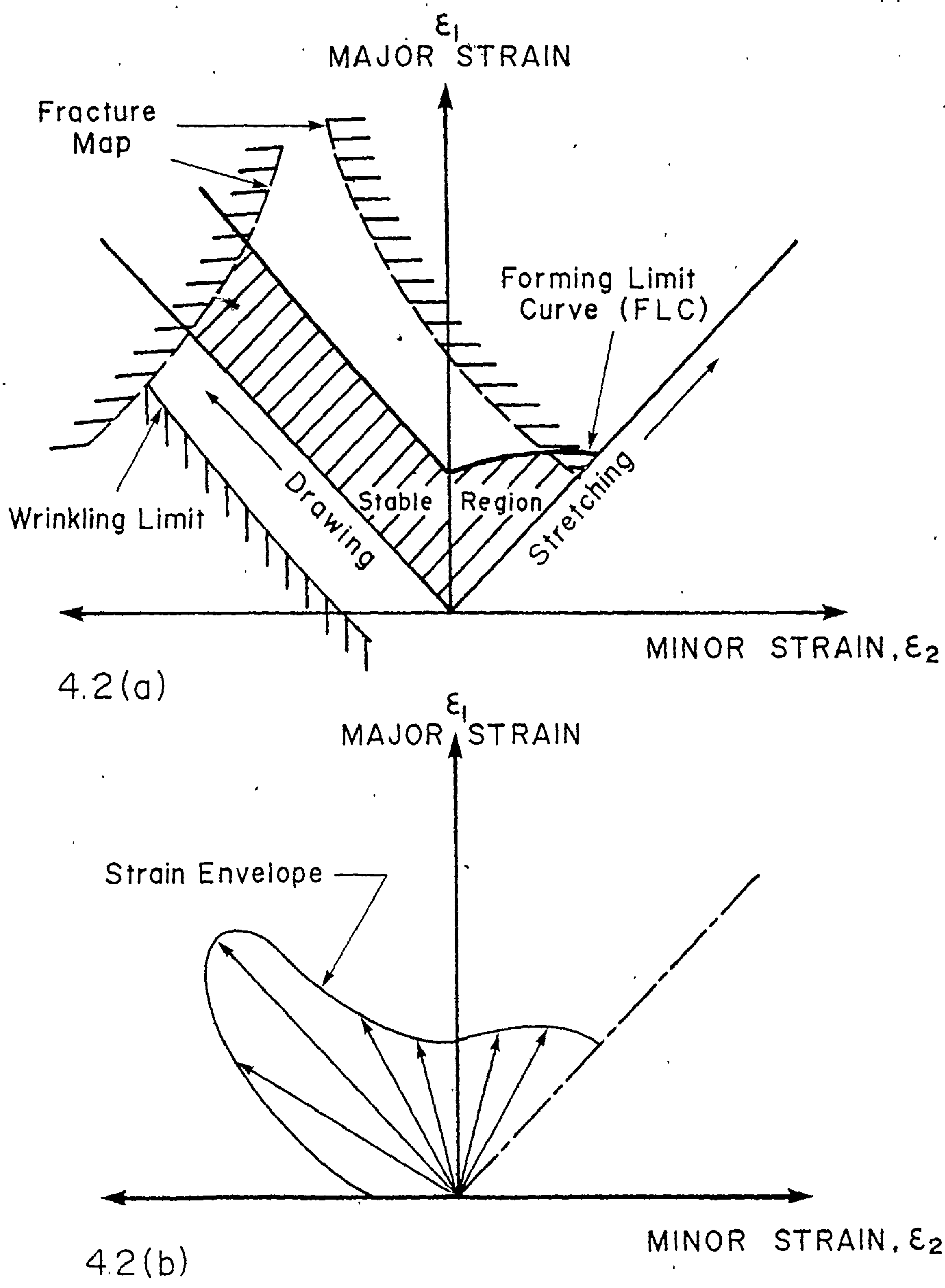

Figure 4.2 (a) A typical forming limit diagram showing the forming limit curve, the fracture map and a wrinkling limit

(b) Envelope of the greatest strain ratios of any linear straining path [33] by failure of any kind. This is then taken as the ideal forming mode because of the reduced possibility of failure.

The concept of geometric modelling may be thought of as finding how a flat sheet can be deformed to cover a particular surface in such a way that every element is deformed in pure shear without change in area and thickness. This is the assumed deformation mode which is employed in the present modelling.

4.3 THEORETICAL BASIS OF THE COMPUTER PROGRAM

To make the analytical model applicable for tool designers in sheet metal forming industries, a computer program called "MAPP" has been developed. The present program has been implemented without access to advanced computer graphics facilities and is generalized so that it can be incorporated into other programs or readily adapted to an interactive computer-aided design system.

A number of flow charts which display the logistics of the model are given in Figures 4.3(a) to (g). These provide a better understanding of the simulating procedures of the process. An explanation of the function of each sub-program and their variable names is given in Appendices D and E respectively. The program developed is by no means a final one, further modifications and improvements are necessary in order to account for other modes.

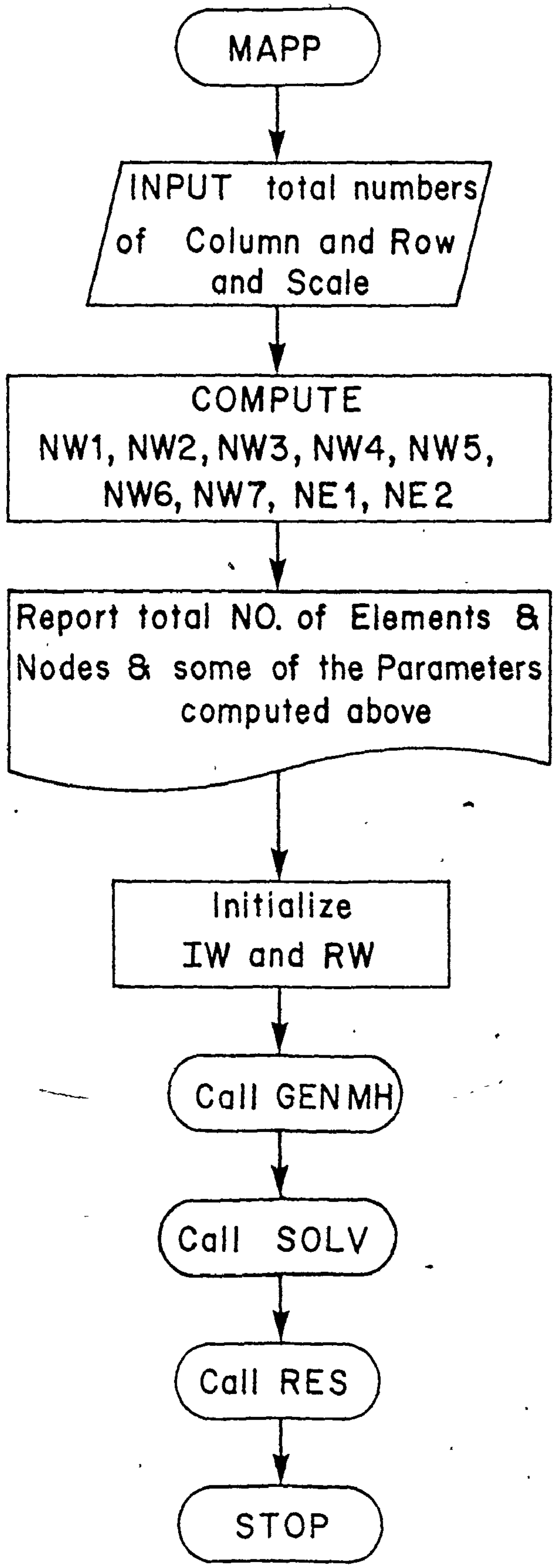

4.3(a)

Figure 4.3 (a)-(g) A complete logistics of the Geometric Modelling Program

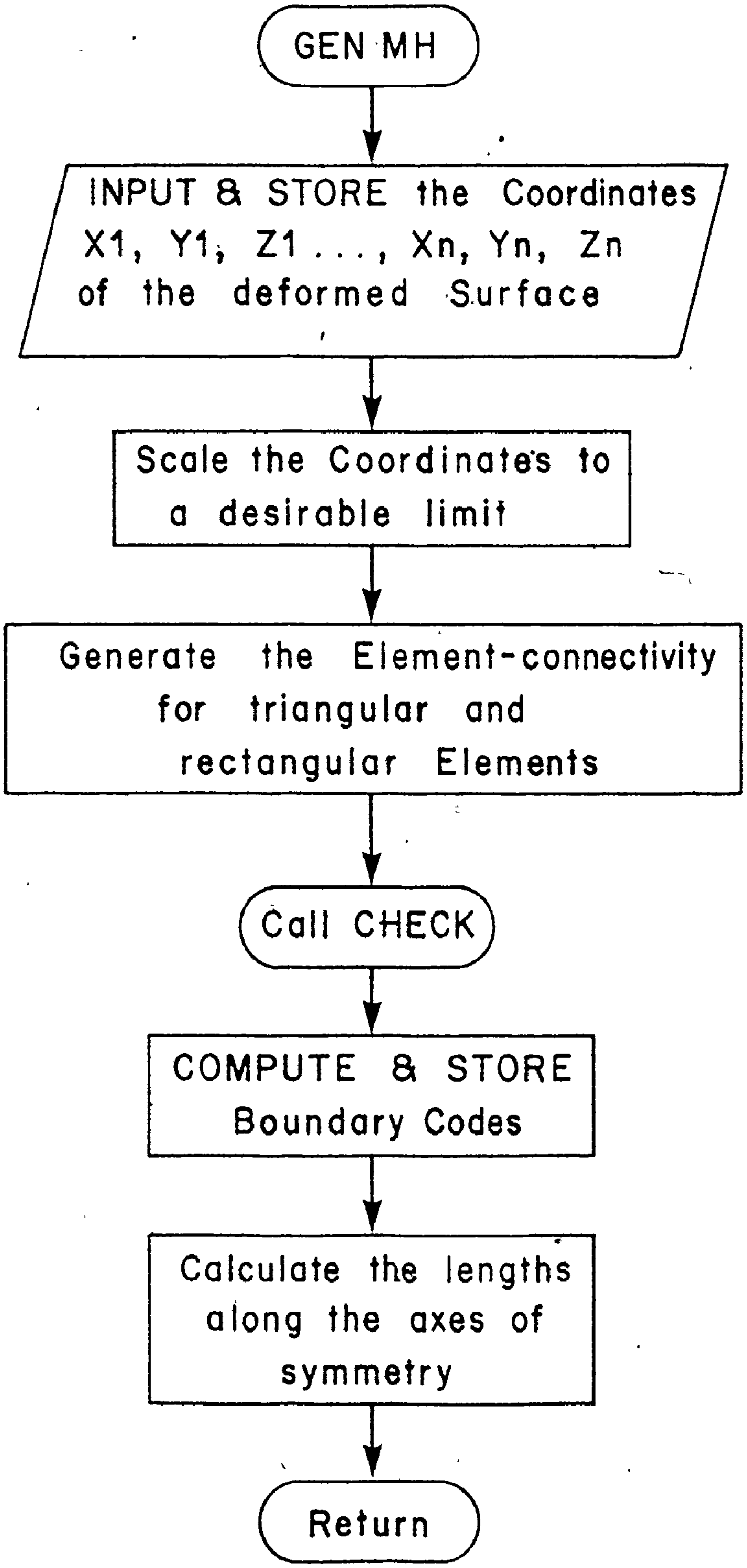
GEN MH
INPUT & STORE the Coordinates X1, Y1, Z1 . . . , Xn, Yn, Zn of the deformed Surface
Scale the Coordinates to a desirable limit
Generate the Element-connectivity for triangular and rectangular Elements
Call CHECK
COMPUTE & STORE Boundary Codes
Calculate the lengths along the axes of symmetry
Return

4.3(b)

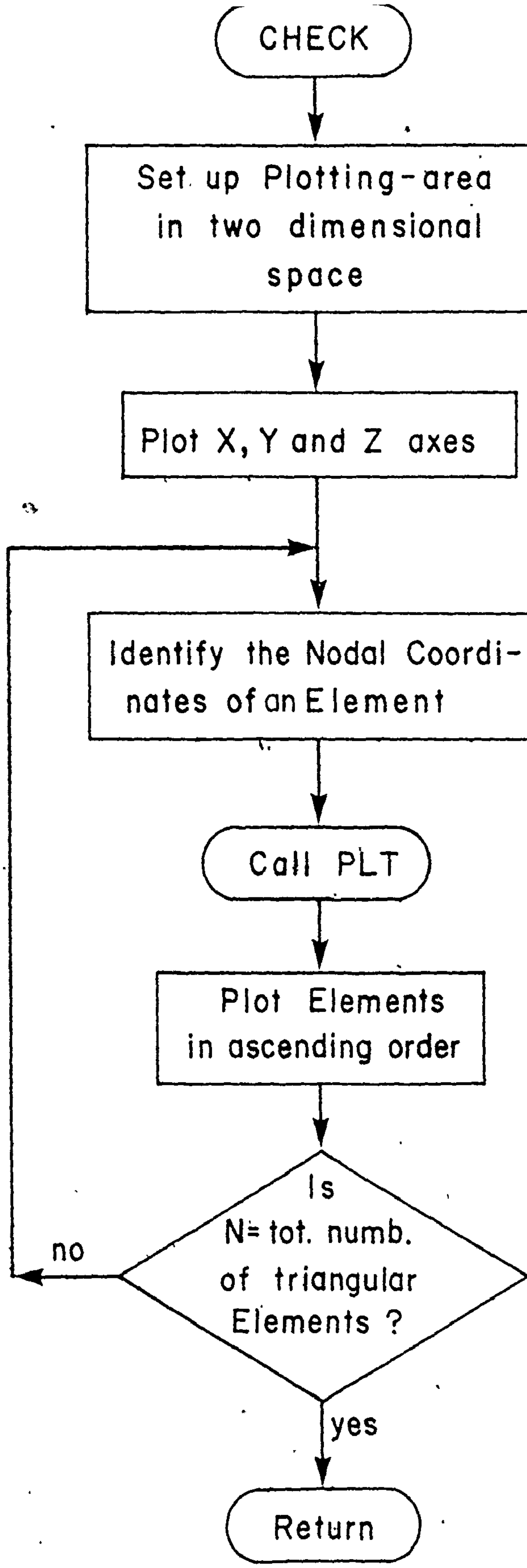
CHECK
Set up Plotting-area in two dimensional space
Plot X, Y and Z axes
Identify the Nodal Coordinates of an Element
Call PLT
Plot Elements in ascending order
Is N= tot. numb. of triangular Elements ?
no
yes
Return

4.3(c)

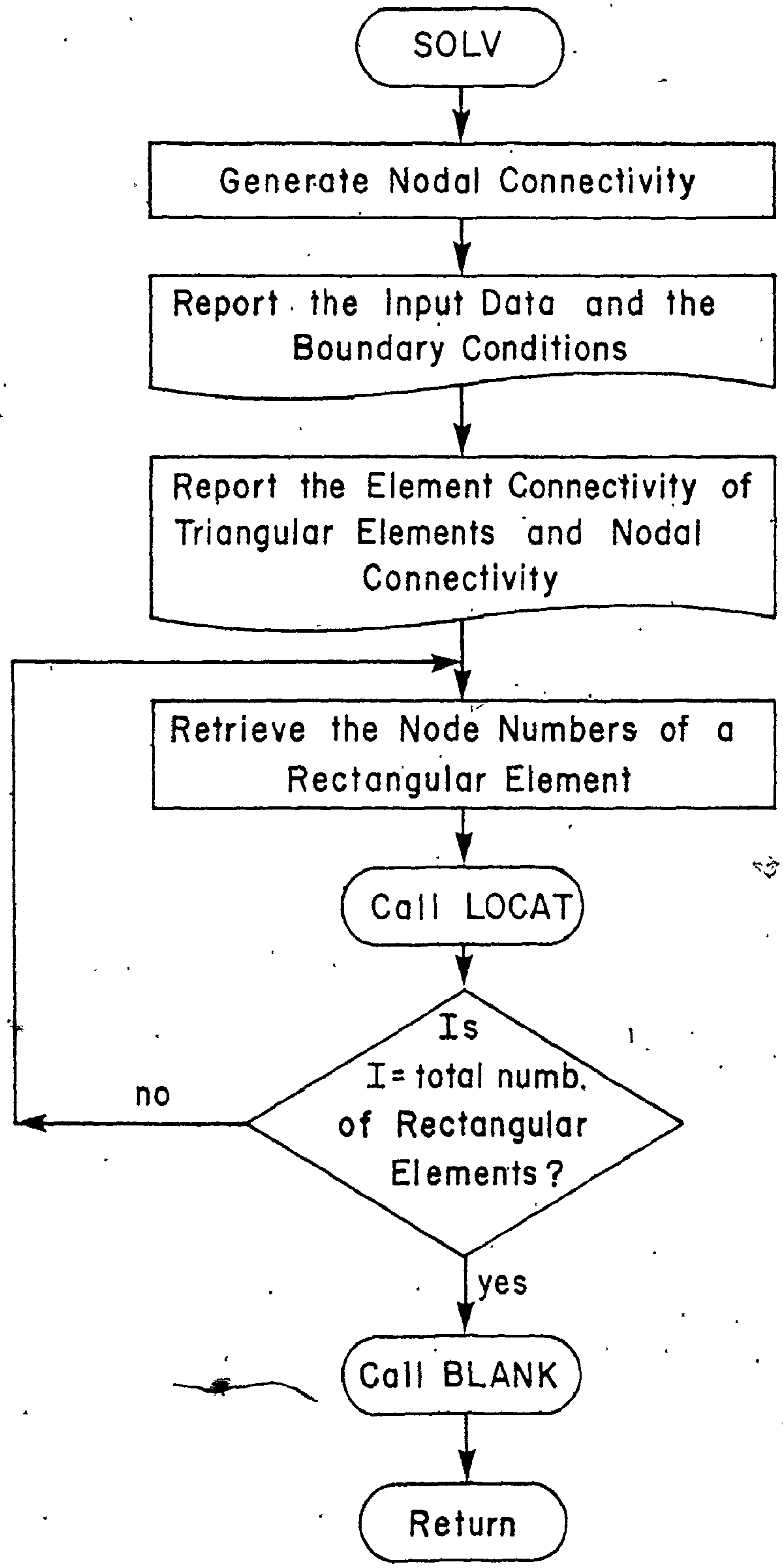
SOLV
Generate Nodal Connectivity
Report the Input Data and the Boundary Conditions
Report the Element Connectivity of Triangular Elements and Nodal Connectivity
Retrieve the Node Numbers of a Rectangular Element
Call LOCAT
Is I = total numb. of Rectangular Elements?
no
yes
Call BLANK
Return

4.3(d)

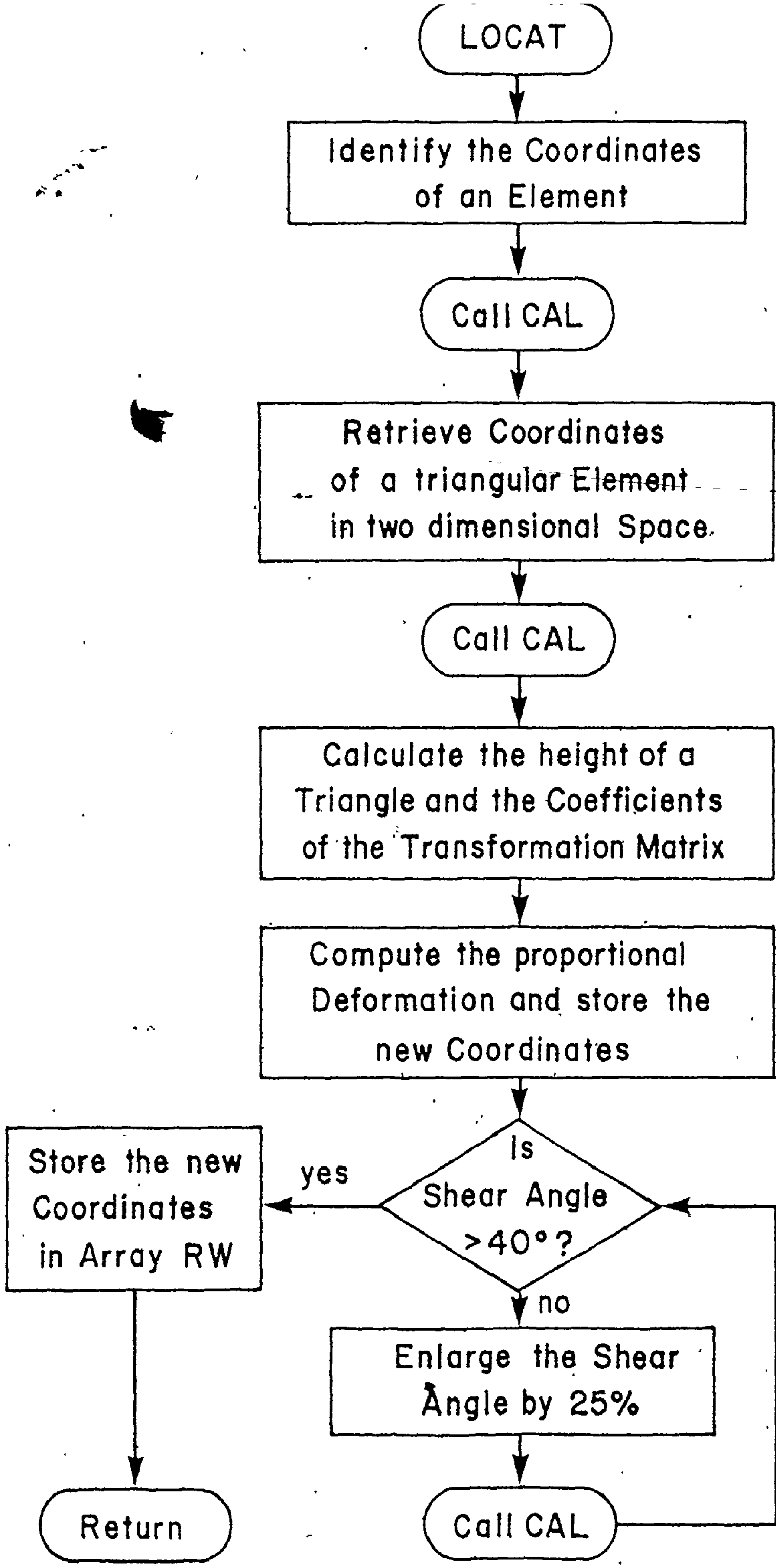
LOCAT
Identify the Coordinates of an Element
Call CAL
Retrieve Coordinates of a triangular Element in two dimensional Space.
Call CAL
Calculate the height of a Triangle and the Coefficients of the Transformation Matrix
Compute the proportional Deformation and store the new Coordinates
Is Shear Angle >40°?
yes
Store the new Coordinates in Array RW
Return
no
Enlarge the Shear Angle by 25%
Call CAL

4.3(e)

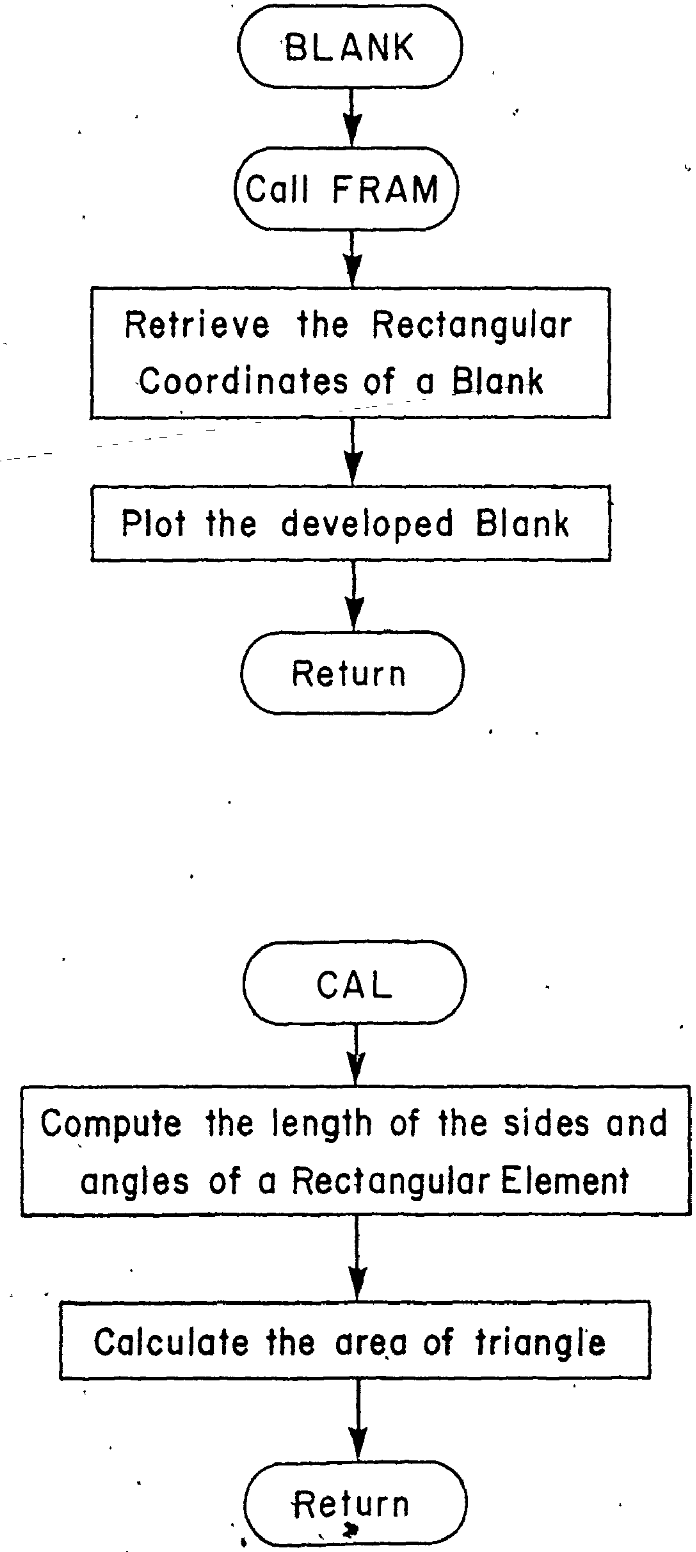
BLANK
Call FRAM
Retrieve the Rectangular Coordinates of a Blank
Plot the developed Blank
Return
CAL
Compute the length of the sides and angles of a Rectangular Element
Calculate the area of triangle
Return

4.3(f)

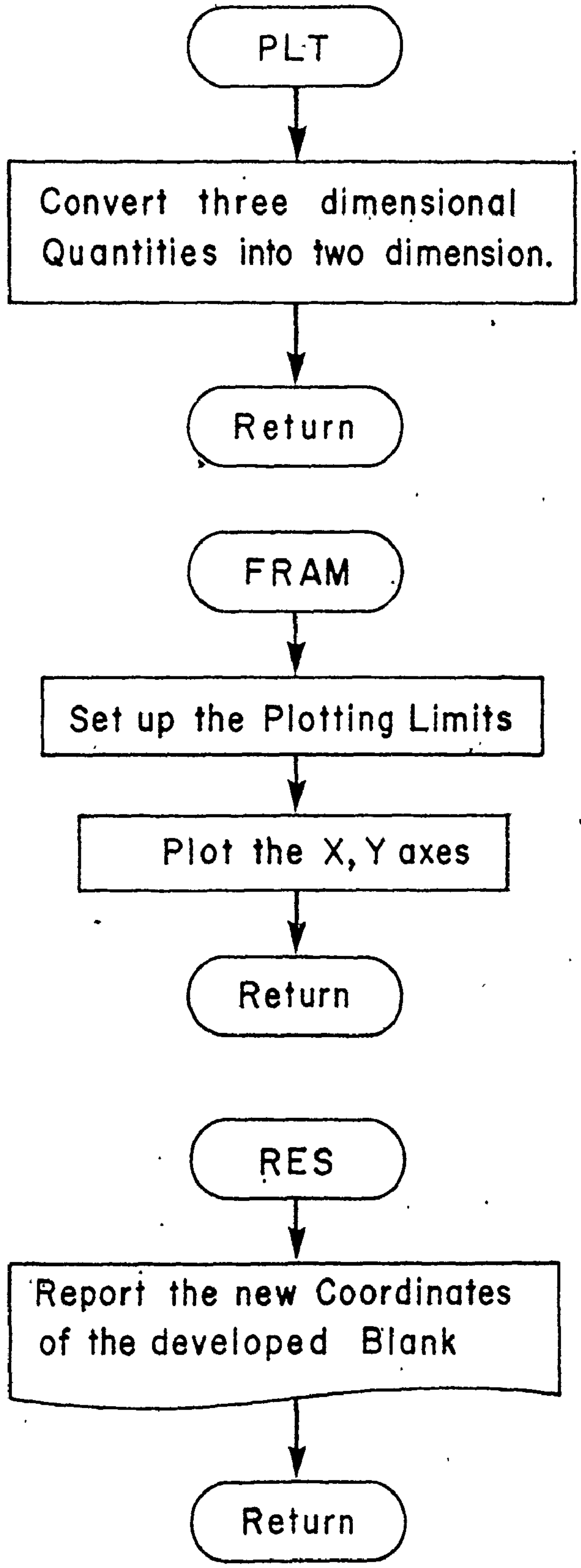
PLT
Convert three dimensional Quantities into two dimension.
Return
FRAM
Set up the Plotting Limits
Plot the X, Y axes
Return
RES
Report the new Coordinates of the developed Blank
Return

4.3(g)

4.3.1 Distance Between Two Points

Line lengths of a stamped surface in three dimensional space are calculated by coordinates of points in the chosen frame of reference, as seen in Figure 4.4.

Applying the Pythagorean theorem to the right angle triangle P_1BP_2, gives

$$(P_1P_2)^2 = (P_1B)^2 + (BP_2)^2$$

$$= (x_2 - x_1)^2 + (y_2 - y_1)^2 + (z_2 - z_1)^2.$$

Hence the distance, d, between points P_1 and P_2 in three dimensional space is

$$d = \sqrt{(x_2 - x_1)^2 + (y_2 - y_1)^2 + (z_2 - z_1)^2} \quad (4.1)$$

4.3.2 Basic Properties of A Triangle

In order to ensure that a triangular element is well defined, its basic properties must be determined completely for subsequent calculations in the program.

The angle θ of a triangle ABC with sides a, b and c, as shown in Figure 4.5, can compute from

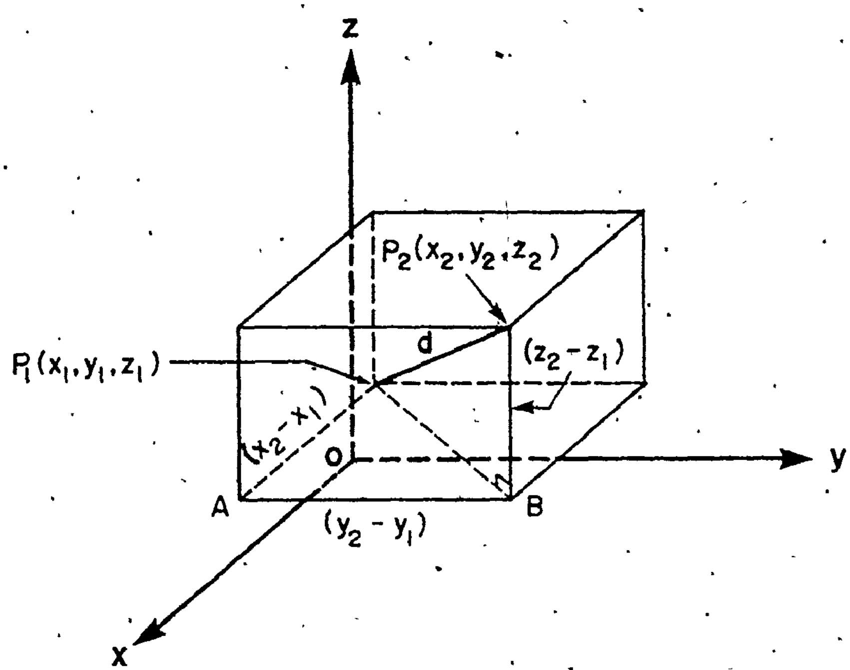

Figure 4.4 A straight line in space which is represented by the diagonal of the element shown

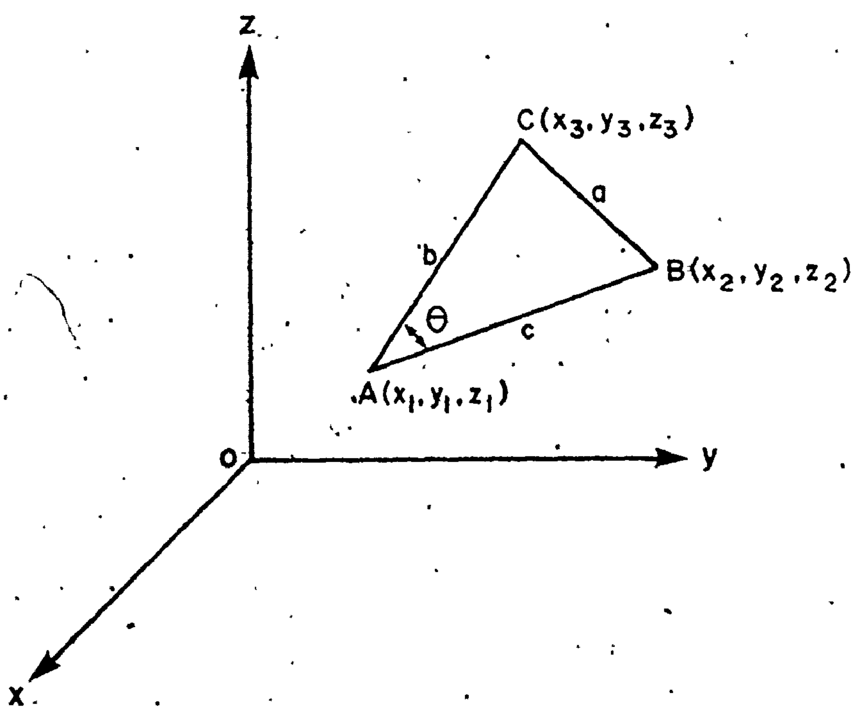

Figure 4.5 A triangular element illustrating its basic properties in three dimensional space

$$a^2 = b^2 + c^2 - 2bc \cdot \cos\theta,$$

or
$$\theta = \cos^{-1} \left[\frac{b^2 + c^2 - a^2}{2bc} \right], \tag{4.2}$$

where
$$a^2 = (x_3 - x_2)^2 + (y_3 - y_2)^2 + (z_3 - z_2)^2$$

$$b^2 = (x_3 - x_1)^2 + (y_3 - y_1)^2 + (z_3 - z_1)^2$$

$$c^2 = (x_2 - x_1)^2 + (y_2 - y_1)^2 + (z_2 - z_1)^2$$

The surface area can be obtained from

$$S = \frac{1}{2} \cdot c \cdot b \sin\theta. \tag{4.3}$$

The above variables are computed by SUBROUTINE CAL.

4.3.3 Proportional Mapping

A quadrilateral element IJKL is assumed to represent a small facet on a curved surface in three dimensional space, see Figure 4.6(a). Assume for the moment that part of the mapping process has been completed and the points i, j and k have been located in the flat plane xoy, as shown in Figure 4.6(b). The area of the triangle ijk is known and the vertical height, h, of the new triangle kil can now be determined, since this must satisfy the condition of equal

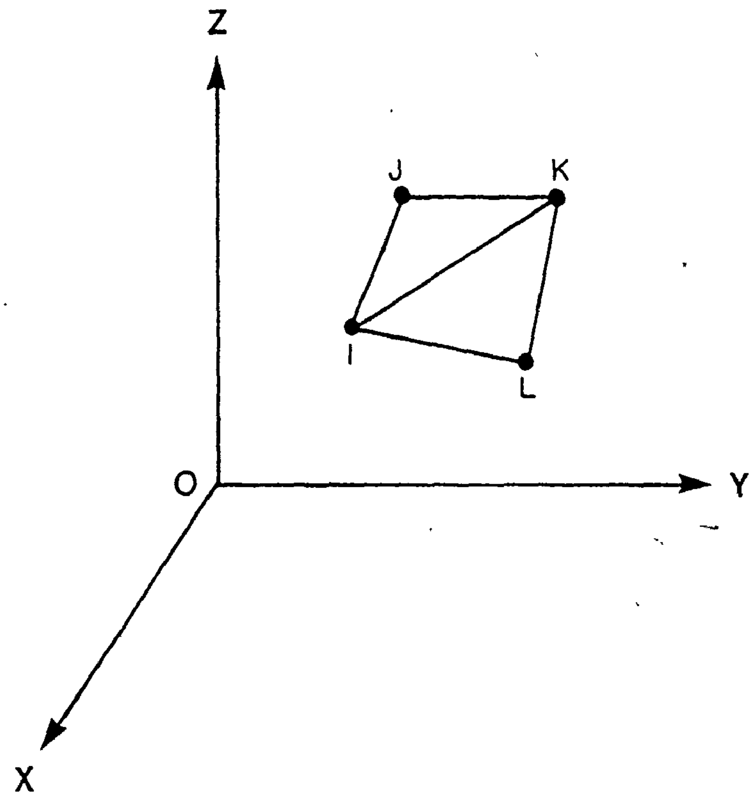

4.6(a)

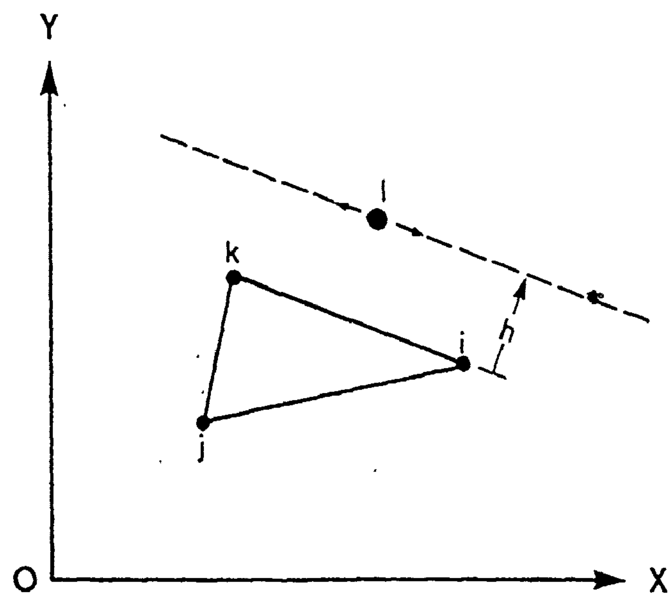

4.6(b)

Figure 4.6 (a) Quadrilateral element on the curved surface
(b) Locating the fourth node in the plane surface

area for the initial and final quadrilateral. The area of the individual triangles IJK and KIL do change in this mapping process but the sum of their areas is constant.

The position of l along the line shown in Figure 4.6(b) must now be found. Proportional displacement is assumed, and this will be apparent from Figure 4.7 where the initial triangle KLI and the final triangle kli are shown superimposed. The position of m along ki is determined by the assumption that the displacement of M will be proportional, such that*

$$\frac{MI}{KI} = \frac{mi}{ki} \tag{4.4}$$

The new node l can now be located with respect to the local frame of reference x'-y', it is then transformed back to the global coordinate axes X-Y by the following transformation. As seen in Figure 4.8,

$$\begin{Bmatrix} X \\ Y \end{Bmatrix} = \begin{bmatrix} \cos\beta & \sin\beta \\ -\sin\beta & \cos\beta \end{bmatrix} \begin{Bmatrix} x' \\ y' \end{Bmatrix} \tag{4.5}$$

where β is the angle of rotation from the local coordinate axes to the global axes.

---

* This assumed mode of deformation minimizes the strain in triangle kli.

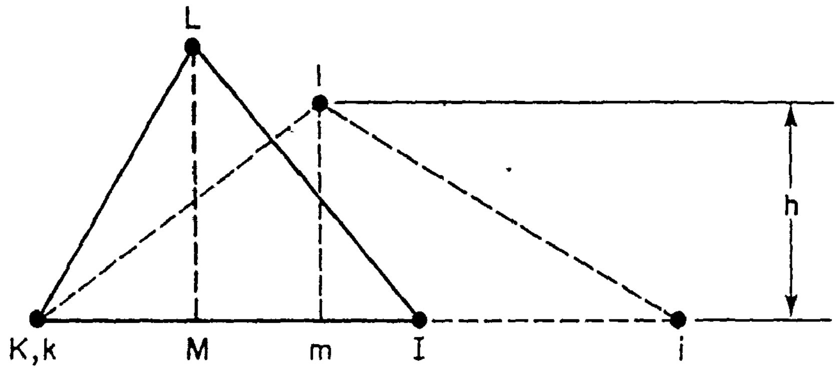

Figure 4.7 Diagram illustrating the assumed proportional deformation

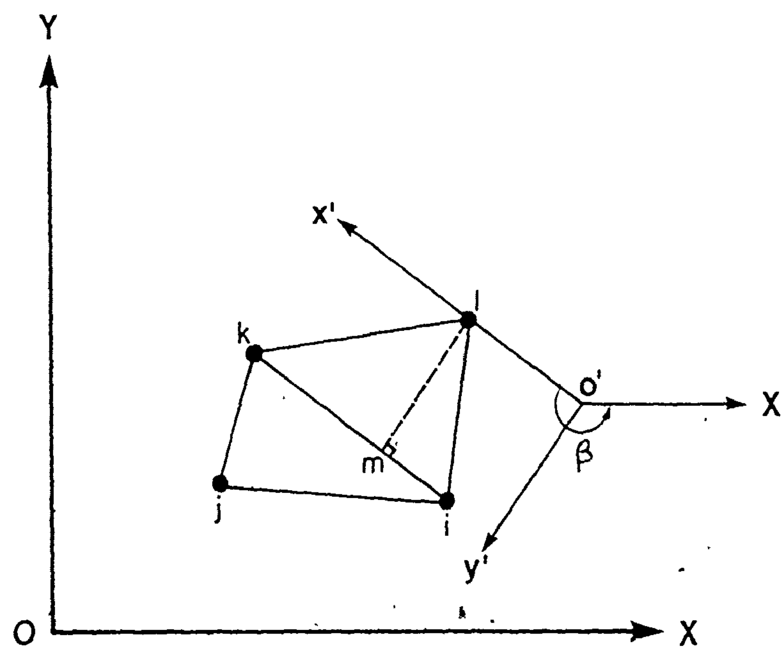

Figure 4.8 Transformation of the fourth node l from the local axes to the global axes

The mapping of other elements is conducted in the same fashion. Several sub-programs have been developed to accommodate these calculations, such as SUBROUTINE SOLV, SUBROUTINE LOCAT and SUBROUTINE CAL.

CHAPTER 5

APPLICATION OF THE MAPPING PROCESS

5.1 INTRODUCTION

In the preceding chapter a proposed geometric modelling technique was discussed in general terms. The assumptions on which the method is based were stated and a brief illustration of the mapping procedure was provided. It is recognised that many of the assumptions are both simplifying and arbitrary and therefore the method is unlikely to produce satisfactory answers for a wide range of industrial pressings. However, it is possible to introduce alternative geometric rules if the ones adopted herein are recognised as being unsuitable to the problem under review.

To test the feasibility of the method, the mapping of two particular surfaces is studied in this chapter. The first study case is that of an analytical surface represented by the equation of an ellipsoid. For the second study case an actual sheet metal component (part of an automobile passenger seat) was employed. As will be seen, the pressing is sufficiently complex in form such as to provide a very realistic test of the method.

5.2 GEOMETRIC MODELLING OF AN ANALYTICAL SURFACE

5.2.1 Mesh Generation

A curved surface which comprises part of an ellipsoid has been chosen for consideration. The surface is described by the equation

$$\left(\frac{X}{6} \right)^2 + \left(\frac{Y}{8} \right)^2 + \left(\frac{Z}{10} \right)^2 = 1. \qquad (5.1)$$

That part of the surface bounded by the planes of symmetry XOZ and YOZ, as shown in Figure 5.1, and within the range of

$$X \in (0,\ 4);\ Y \in (0,\ 4) \text{ and } Z \geq 0,$$

is isolated for analytical purposes.

A topologically rectangular mesh is generated to cover this surface as shown in Figure 5.1. In the analysis, the surface is approximated by the contiguous triangular elements and each quadrilateral element is folded along one particular set of diagonals. The generated mesh serves as an initial error check of the input data. SUBROUTINE CHECK has been developed for such a purpose, and it employs the Versatec 1200A plotter to generate the required mesh.

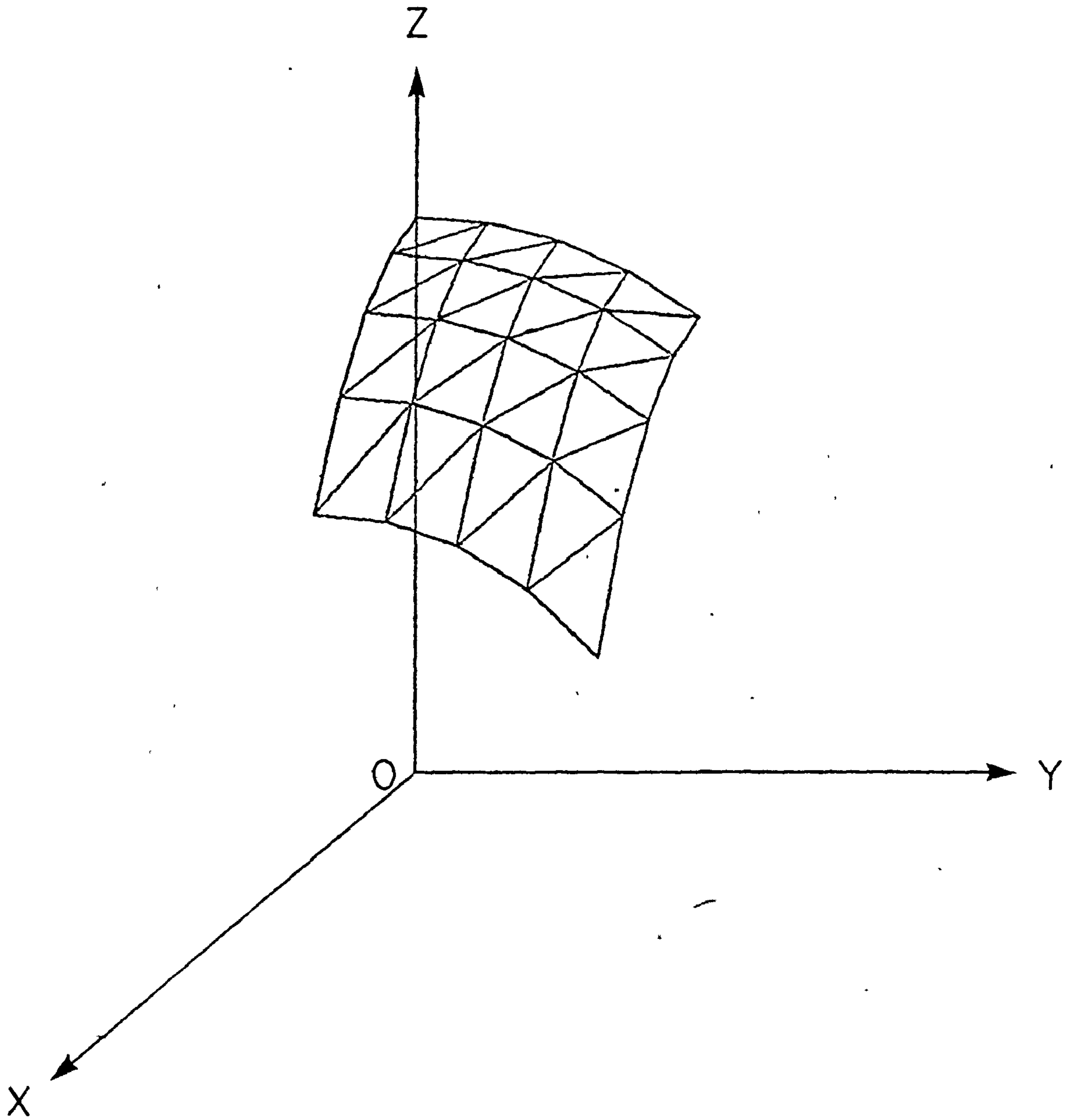

Figure 5.1 Portion of an ellipsoidal surface which is modelled by a 4x4 mesh

5.2.2 Boundary Conditions and Proportional Transformation

Some appropriate displacement boundary conditions must be specified for certain nodes. In this case, planes XOZ and YOZ are planes of symmetry and hence the component of displacement perpendicular to these planes will be zero. In the present example it is also specified that the distance between these boundary nodes does not change, i.e. the sheet deforms without extension along these lines of symmetry. This particular boundary condition is an arbitrary one. If the designer considers that the spacing between the nodes changes along the axes of symmetry he can impose such a condition; hence the designer may change the input conditions in light of his own experience.

The boundary nodes can now be mapped in the XOY plane as illustrated in Figure 5.2. There must always be a starting point in which three vertices of a quadrilateral have been fixed at the intersecting corner of the axes of symmetry. The problem now is to map each of the nodes onto a flat plane such that the quadrilateral elements remain of constant area and that the continuity of the elements is maintained.

The mapping can proceed in a number of ways and three possible sequences are illustrated in Figure 5.3. In the present anlaysis the free nodes are located by diagonal traverses only, as indicated in Figure 5.3(c). The general

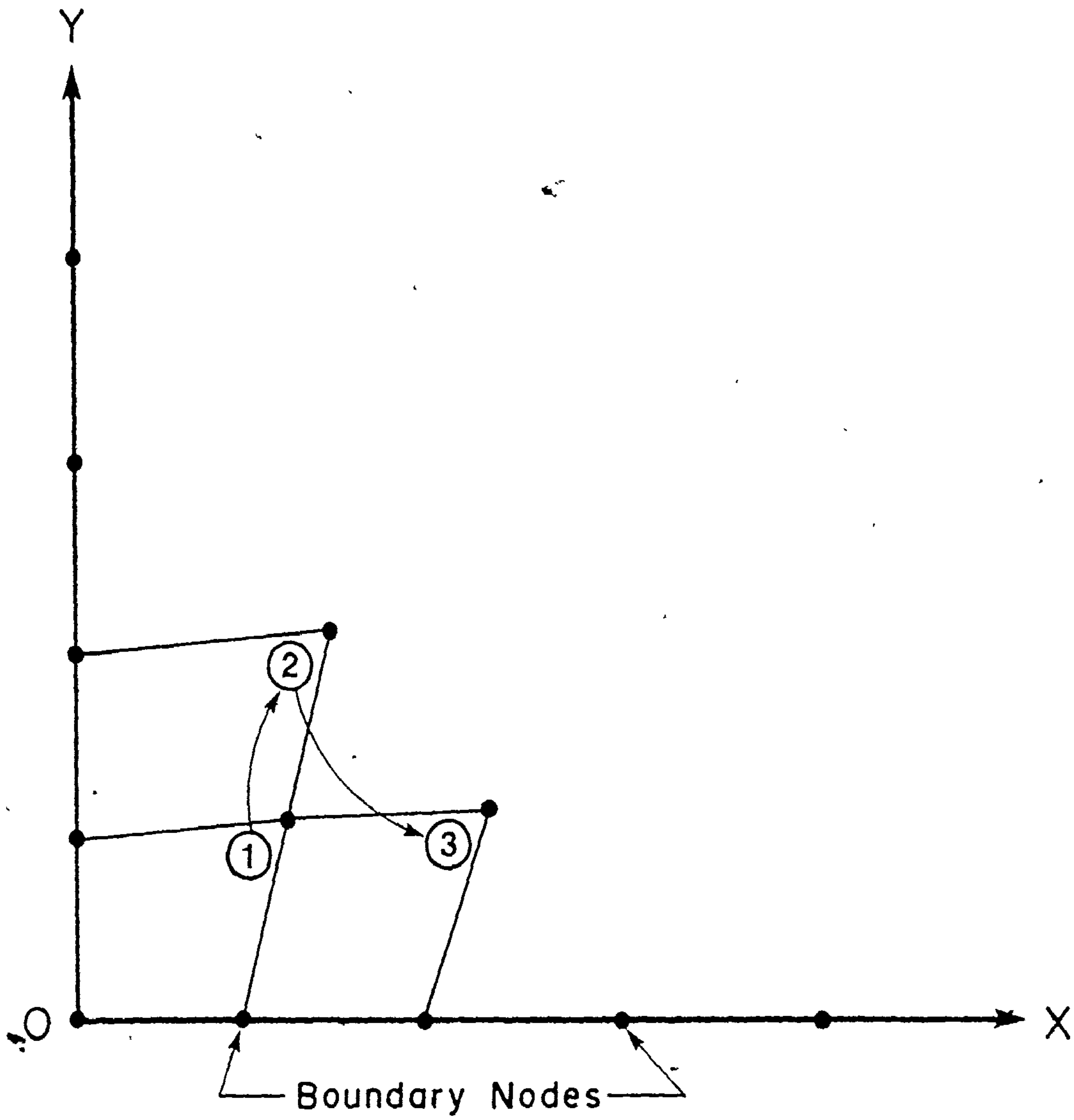

Figure 5.2 Diagram showing the boundary nodes and the order of mapping of each element which is employed in the analysis

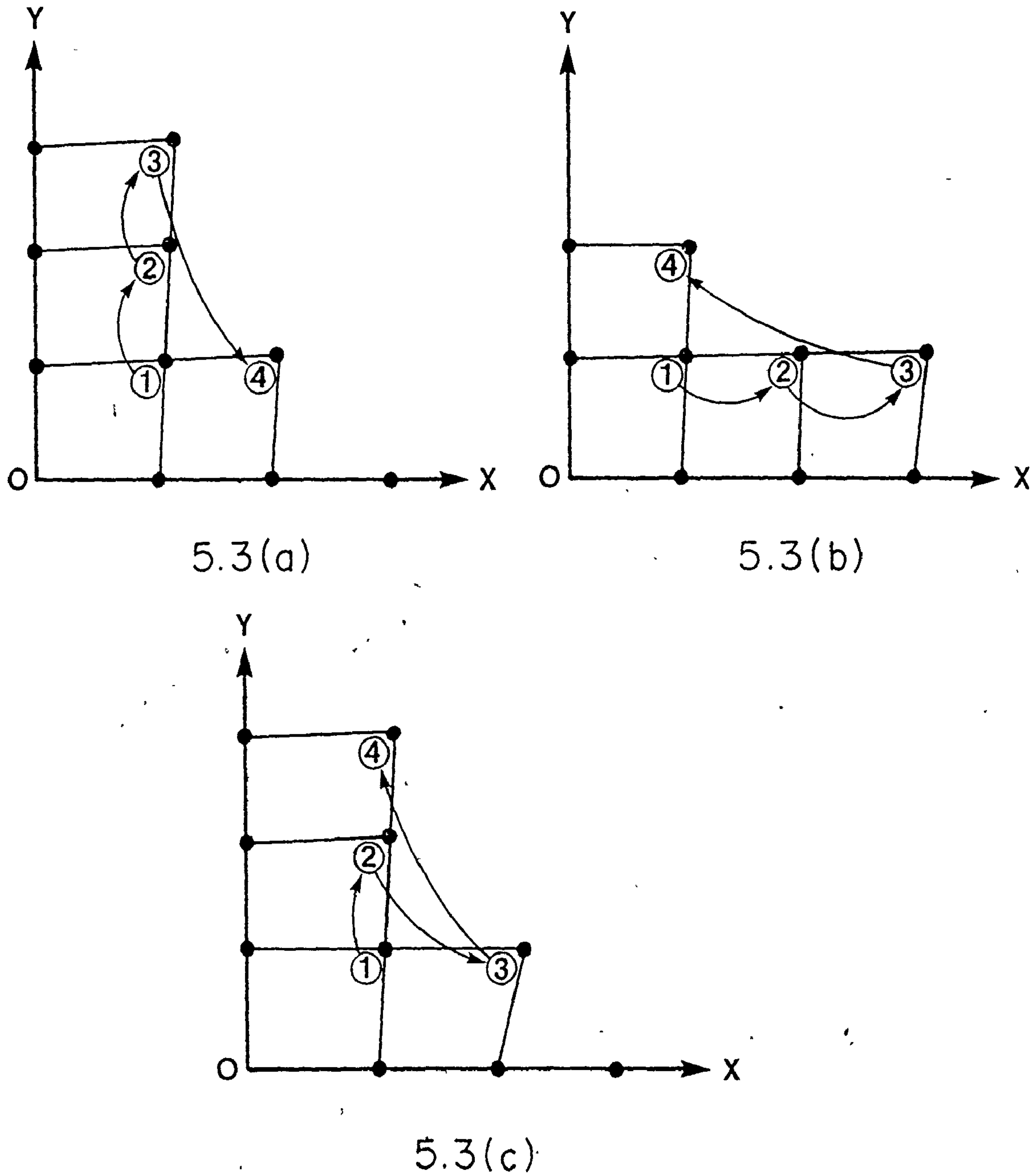

Figure 5.3 Mapping sequence for locating the fourth node of a quadrilateral element
(a) Column-wise mapping
(b) Row-wise mapping
(c) Diagonal traverses

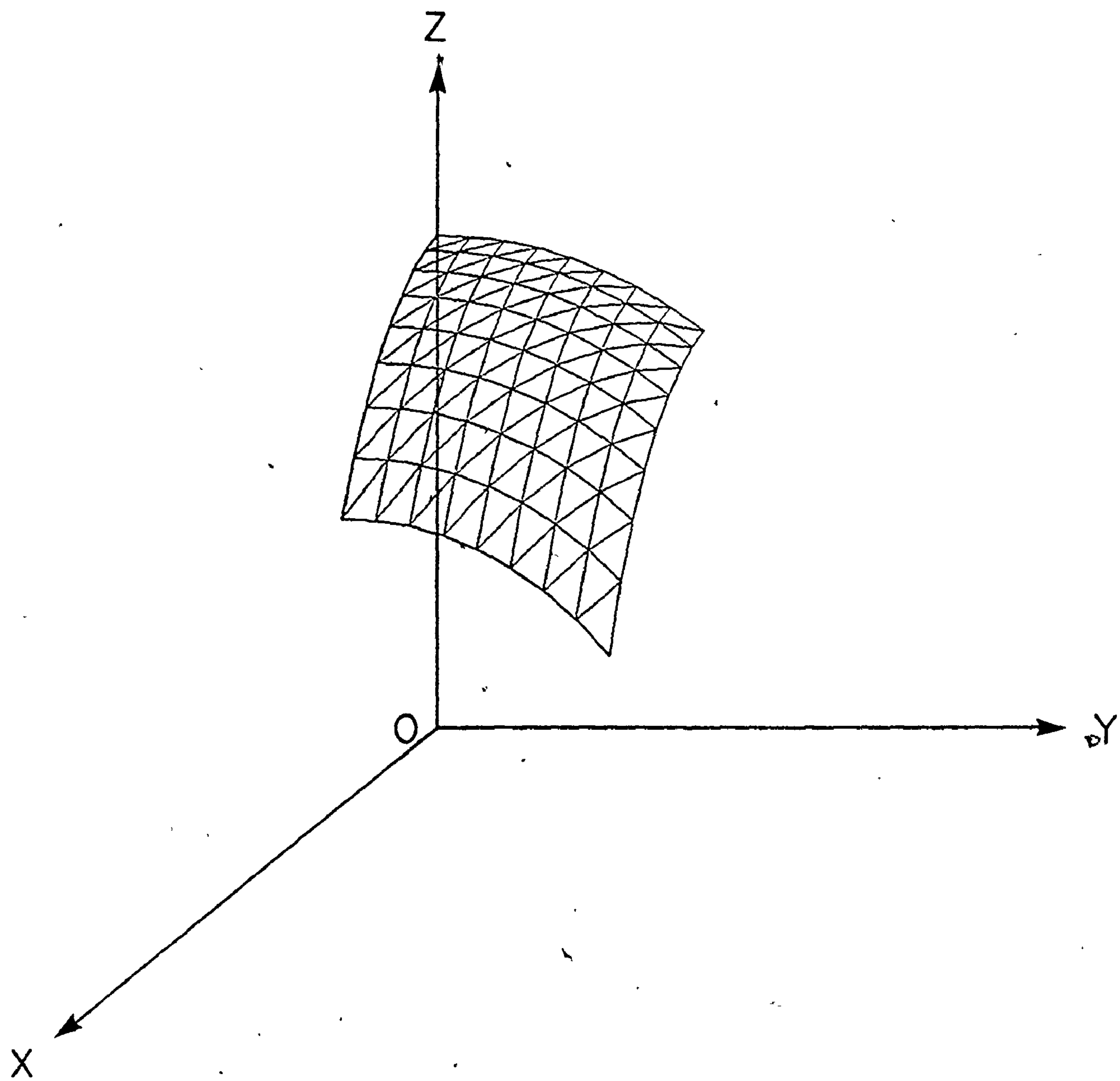

Figure 5.4 The same portion of the ellipsoidal surface which is now modelled by a finer 8x8 mesh

procedure for locating the fourth node of a quadrilateral element follows exactly the same procedure outlined in section 4.3.3 of the previous chapter.

With the same strategy of proportional deformation, equation (4.4) can be expressed in terms of elongation of point M. A different way of interpretation of the proportional deformation can be observed, again from Figure 4.7 the following expression is deduced, i.e.

$$\frac{\overline{Mm}}{\overline{Ii}} = \frac{\overline{KM}}{\overline{KI}} \qquad (5.2)$$

The free node can now be located and transformed back to the global coordinate axes using equation (4.5), and the next element is mapped in the similar manner.

5.2.3 Results of the Mapping Process

The result of the mapping process for the surface shown in Figure 5.1 is given in Figure 5.5(a). The practical importance of this is that the flat shape shown in Figure 5.5(a) could be considered as an initial blank. This blank, at least theoretically, can be made to conform to the ellipsoidal surface in Figure 5.1 in such a way that the criteria imposed above are satisfied. It should be noted that the blank generated in Figure 5.5(a) is not the only one which would satisfy the imposed conditions but it is a

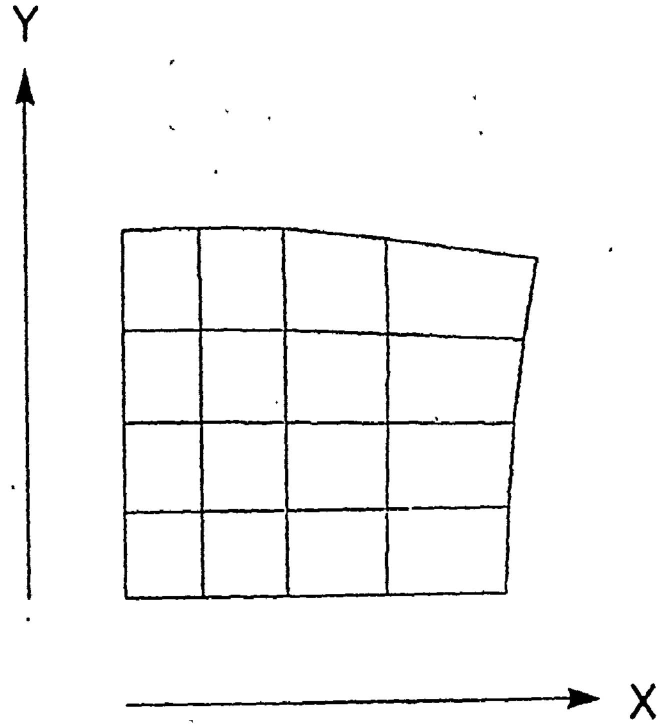

5.5(a)

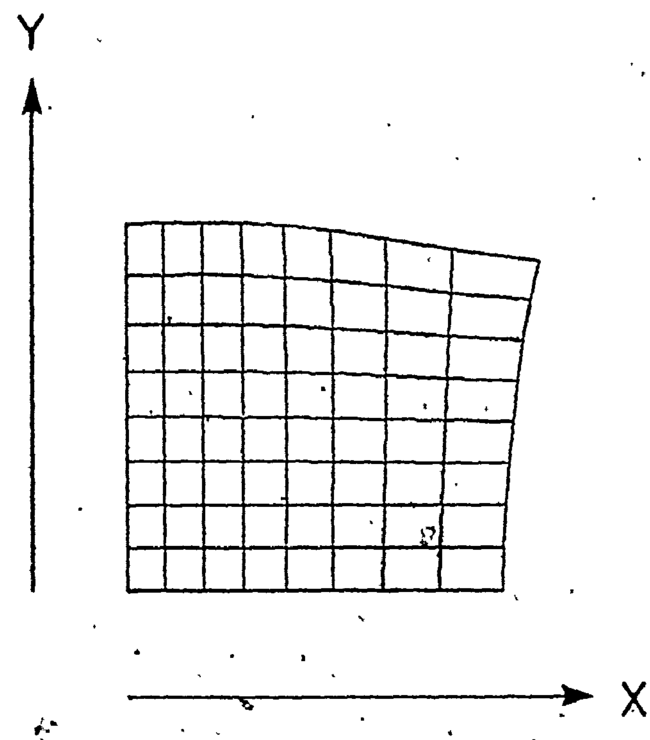

5.5(b)

Figure 5.5 (a) The resulting transformation of the ellipsoidal surface shown in Figure 5.1
(b) The resulting transformation of the same ellipsoid using a finer m[illegible] in [illegible] 5.4

possible one. Obviously if different geometric rules are incorporated into the analysis then a different blank shape would ensue.

A more refined mesh with 128 triangular elements has been applied to cover the same ellipsoidal surface; this mesh provides a better and closer approximation to the true geometry of the surface, as shown in Figure 5.4. The same mapping procedure is employed to transform the elements onto a flat plane. The result of the transformation for this surface is shown in Figure 5.5(b). In this case there is no significant difference between the resulting transformation, as can be seen from Figures 5.5(a) and 5.5(b).

However, for parts with a more complex geometry it may be advisable to employ a finer mesh in order to provide a better representation of the surface.

5.3 DISCUSSION

Two mesh sizes, shown in Figures 5.1 and 5.4, were employed in the transformation of the ellipsoidal surface to a plane. The results of the mapping are shown in Figures 5.5(a) and 5.5(b). It will be appreciated that the finer mesh provides a better representation of the curved surface, and in turn the generated flat blank possesses a smoother contour. However, as can be seen from Figures 5.5(a) and (b) the developed blanks are very similar in appearance.

Each of these blanks can be deformed, at least in principle, to the ellipsoidal surface such that the predicted strain distribution is geometrically compatible with the constraints imposed by the designer. This strain distribution may not be one which is entirely possible physically; it is only kinematically acceptable. The author believes that the higher the order of approximation, i.e. the larger the numbers of elements, the better the results and the closer and more accurate the correspondence of the strain distribution to reality.

The mesh size does have an effect, but it is not critical in the current example. The method seems to be highly successful in transforming the ellipsoidal surface into a flat sheet. A more stringent test of the method is presented in the next section where the surface under investigation is part of an actual pressing and is not smooth and regular.

5.4 MODELLING OF PART OF A STAMPING

The corner of a passenger car seat stamping was then selected for study. The metal blank had been gridded with circles prior to forming, and upon examination of the deformed part it was observed that a corner of the pressing could be isolated for study, i.e. there existed two orthogonal planes across which the displacement was negligible.

5.4.1 Mesh Generation

A grid of quadrilateral elements was drawn freehand on the part using a marker pen. The only restriction was that the elements should be topologically rectangular, i.e. they should form the required rectangular array of rows and columns. A photograph of the original stamping, from which the corner section was removed, is shown in Figure 5.6(a). Figure 5.6(b) shows a photograph of the piece removed from the corner for modelling. The grid of lines marked on the surface of the component are clearly visible in the photograph.

The part was then placed in a coordinate measuring device and the location of the vertices of the hand-drawn quadrilateral elements was recorded. The readings were taken with respect to a fixed cartesian reference frame and the data points stored in a computer. A reconstituted picture of the mesh, using a 1200A plotter is shown in figure 5.7; the diagram provides a visual check on the digitizing. As part of the plotting routine the diagonals of the quadrilaterals were inserted on Figure 5.7.

The boundaries of the part are located on the planes of symmetry XOZ and YOZ, and as before the displacement of

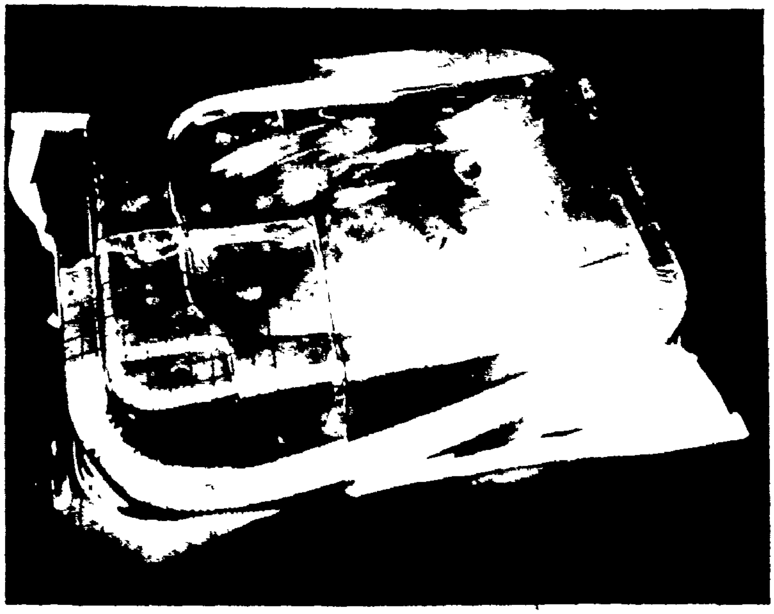

5.6(a)

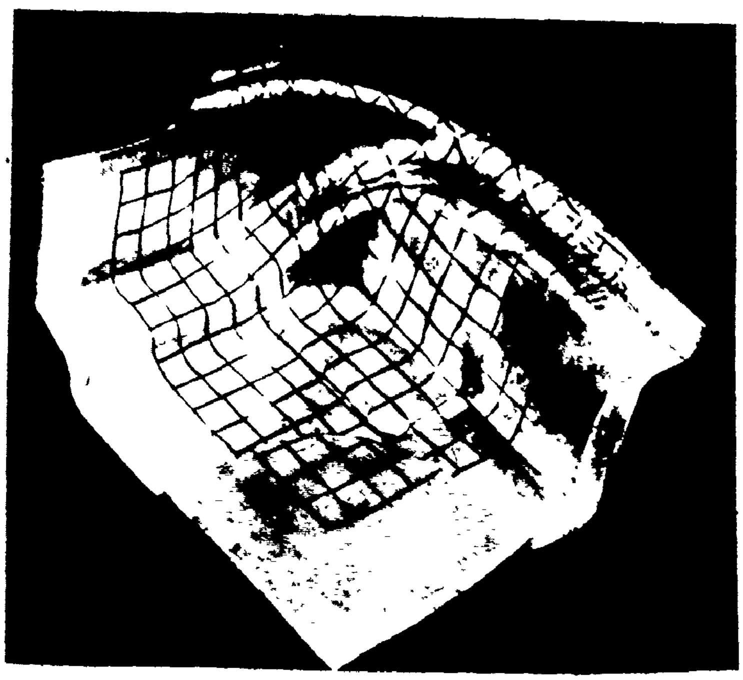

5.6(b)

Figure 5.6 Photographs: (a) of a seat stamping and
(b) the area removed from the corner for modelling

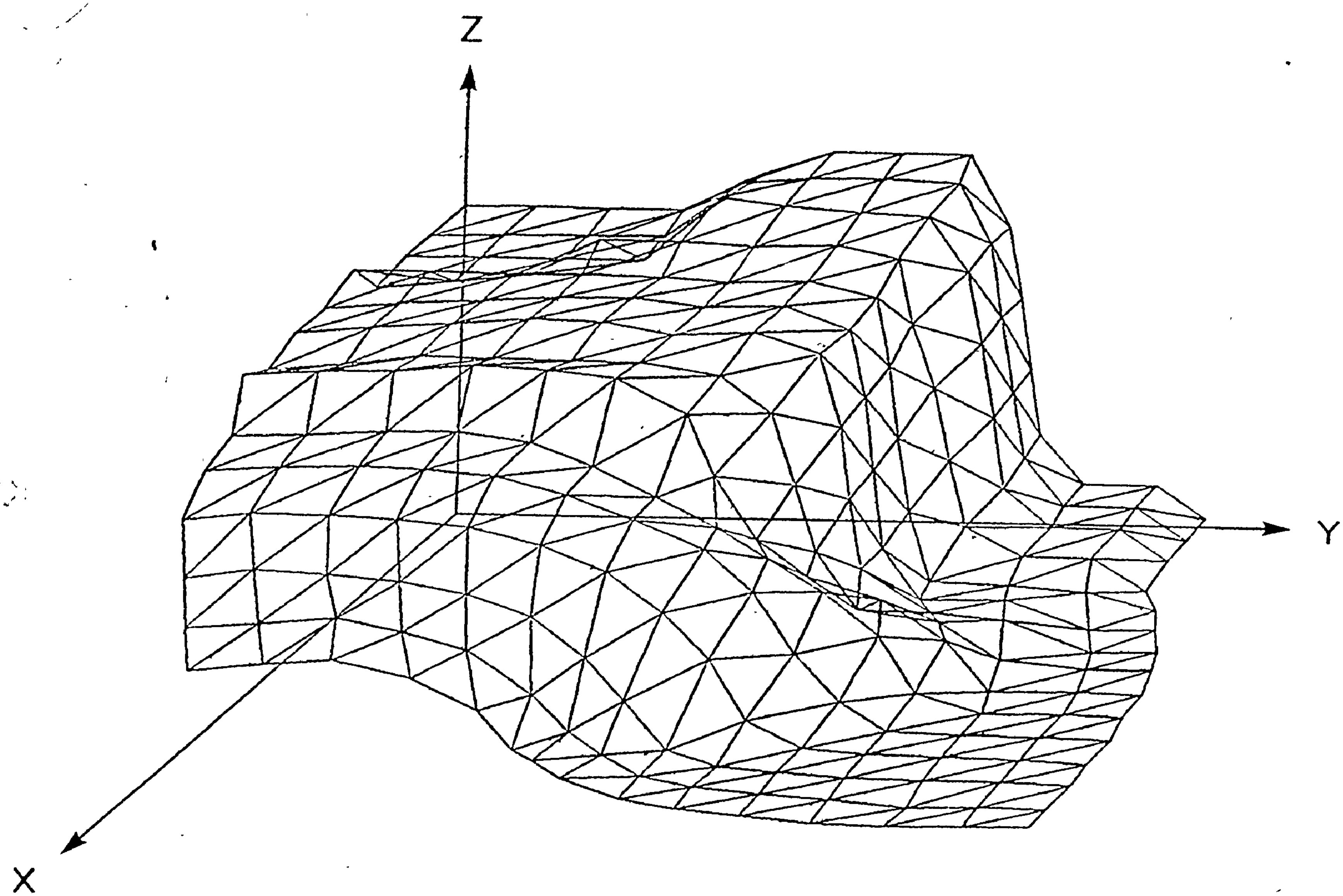

Figure 5.7 Mesh obtained from the region shown in Figure 5.6(b)

the nodes along the lines of symmetry can be specified. For the part under inspection it was found that the length changes between the nodes along the axes of symmetry was, in the main, negligible. The nodal positions along the OX and OY axes in the plane were therefore readily established. The mapping procedure was then carried out in the same manner as that already described. In the present case each of the three mapping sequences of Figure 5.3 was employed to ascertain what effect this might have.

5.4.2 Results of Mapping

It transpired that the mapping sequence had negligible effect* on the final shape of the flat blank, hence only the results obtained by diagonal traverses are presented. The result of the mapping procedure is shown in Figure 5.8. The uneven edge at the top and right hand boundary suggests that the modelling is not very realistic. A more serious problem is the overlapping of elements in the vicinity of the upper right hand corner, and points to an unacceptable instability in the mapping process. It is interesting to observe that the non-conforming elements occurred in a region where the trial stampings showed severe wrinkling.

The existing mapping procedure, although found wanting, may serve as a warning system at the preliminary

---

* The three mapping secuences of 5.

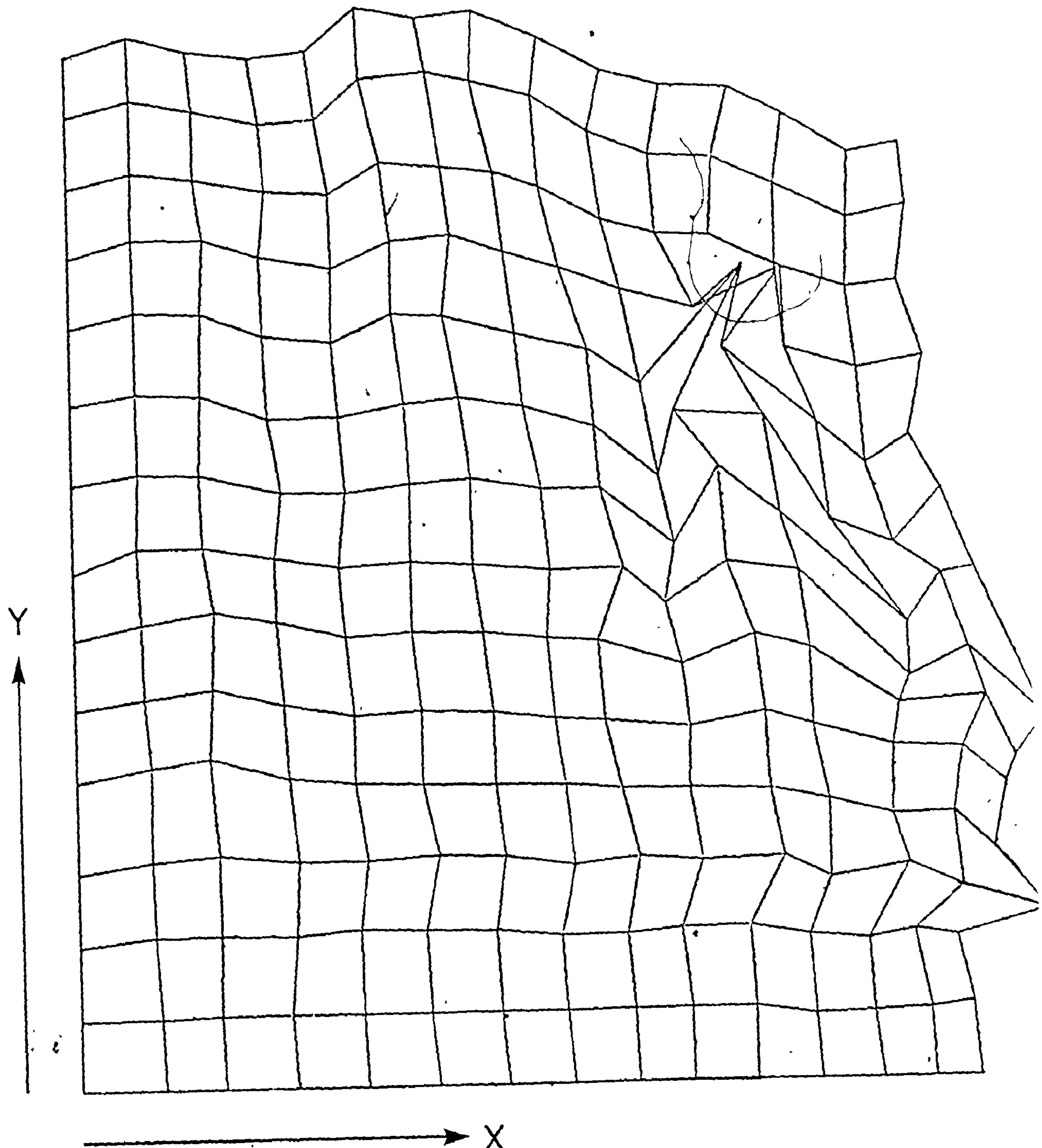

Figure 5.8 Transformation of the mesh in Figure 5.7 into the flat plane showing the area of instability

design stage. The appearance of non-conforming elements would imply that large surface area changes are likely to take place in the actual pressing with the possibility of failure by wrinkling or tearing. The mapping procedure will have to be performed on an additional number of industrial pressings before the preceding ascertion can be justified.

The non-conforming elements indicate that there is a deficiency in the imposed geometric strategy, i.e. the requirement that the deformed and undeformed quadrilateral elements maintain the same surface area, and the mapping process which serves to satisfy this hypothesis. The instability in the mapping technique becomes evident when individual quadrilaterals begin to develop very acute or obtuse included angles. This often resulted in the two triangular regions making up the quadrilateral, showing very different surface areas*.

In an attempt to overcome this difficulty, an arbitrary limit was imposed on the change in the apex angle of any triangle during the mapping process. This tended to dampen out severe changes in the shape of a triangular element, and a preliminary result is shown in Figure 5.9. This is free from overlapping but deficiencies are still evident.

---

* A possible physical interpretation is the existence of a region(s) of high strain gradient on the pressing.

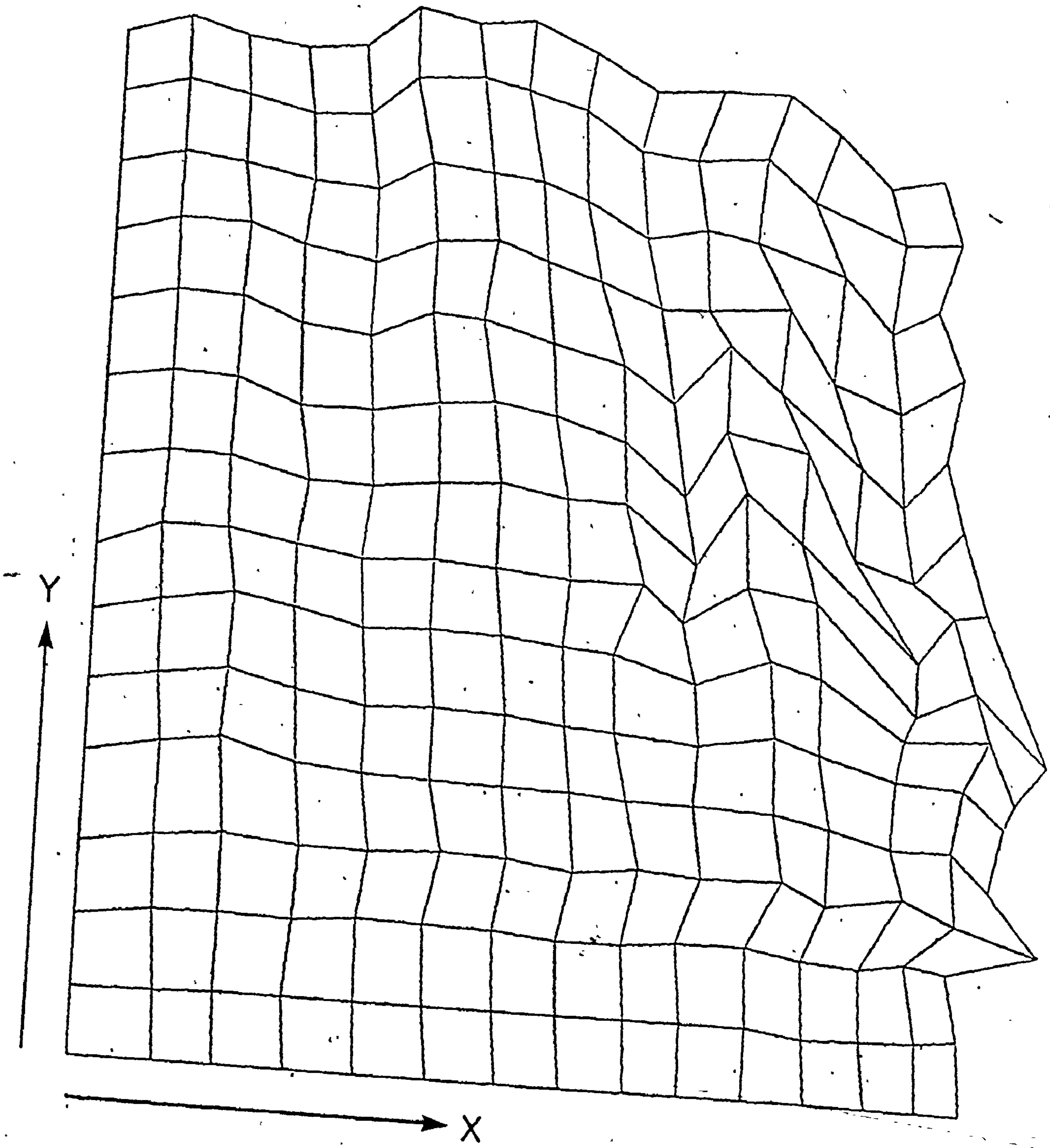

Figure 5.9 An improved transformation into the plane

5.5 DISCUSSION

The corner of a passenger seat stamping shown in Figure 5.6(b) was modelled, using a 14 x 14 quadrilateral mesh. The results have exposed deficiencies in the proposed mapping procedure, the most serious of these being non-conforming elements. There are probably three explanations for this phenomenon:

(i) The array of grids which were drawn freehand on the stamping are highly irregular, particularly in the regions of drawing-in and re-bending. These produce large errors in the calculations of the basic variables of a triangle. In fact, any extreme irregularity between an element and its neighbouring facets, it is likely to cause overlapping of elements during the transformation process.

(ii) It was mentioned in Section 5.2.3 that the mesh size is likely to play a more important role when attempting to represent the surface geometry of a complex pressing. It can be seen from Figure 5.7(b) that the hand drawn elements are relatively large. Better results might have been obtained if smaller elements had been employed, particularly in the regions where sharp bends were present. Further work needs to be performed to verify the preceding remark.

(iii) Finally, it is doubtful whether the modelling procedures adopted here can ever adequately describe the deformation undergone by such a complex part. It may be necessary to impose other criteria in order to improve the performance of the mapping process.

The pressing selected for study in this section is reasonably complex in shape, and therefore provides a very realistic test for the geometric modelling technique. Certain deficiencies in the technique have been revealed and it may be necessary to modify the present strategy. However, the author believes the modelling procedure possesses many of the ingredients which will aid the designer, if an appropriate strategy can be determined. The execution time for the mapping procedure is very quick. In the present case it took only a few seconds on the McMaster CDC 6400 central computer to provide the results shown in Figures 5.8 and 5.9.

CHAPTER 6

CONCLUSIONS AND SUGGESTIONS FOR FURTHER WORK

CONCLUSIONS

A technique has been developed for the determination of the magnitude and direction of the principal strains from measurements performed on a deformed grid of lines. The method is applicable for the assessment of the strain distribution on the surface of the sheet metal pressing, where a grid of lines e.g. a pattern of either squares, rectangles or parallelograms, has been previously marked on the undeformed blank. (It is standard practice to photographically print or electrochemically etch grid patterns on sheet metal blanks for subsequent strain determination in press shop trials.)

The technique is strictly applicable to a homogeneous deformation mode, where straight lines are deformed into straight lines without rotation of the principal strain axes with respect to the material element. As remarked in the text the entire surface of a sheet metal component is unlikely to follow this type of deformation, but there may be many regions on the pressing which, to a good approximation, obey this mode of deformation. It is to be noted that a homogeneous deformation mode is implicit in the widely employed "grid circle method". The undeformed grid is assumed to deform into an ellipse and the principal strains are determined by measuring what are deemed to be the major and minor diameters.

The present method improves upon the accuracy of the grid circle method, since if a grid circle circumscribes a square, then measuring the deformed pairs of sides leads to both a better averaging procedure and the assessment of the maximum strain values.

The analytical procedures have given rise to a symmetric second order finite strain tensor. This is simpler in form than the finite strain tensor (GREEN or FINGER) defined in many texts on Continuum Mechanics. The present analysis does not rely on tensor algebra *per se*, and this should prove to be a welcome simplification to many engineers who frequently encounter difficulty with the notation and also the concepts, particularly when finite deformatons are being discussed.

Another aspect of the present work has been an attempt to provide a technique to aid in blank development for complex press-formed parts. The starting point is the specification, by the designer, of the *final* shape of the component. Herein a first attempt has been made to establish a procedure for transforming or mapping the deformed component back to an undeformed blank shape. The mapping procedure is assumed to obey certain geometric rules only, and the present work has concentrated on an equal area hypothesis.

The technique appeared to work quite well on a deformed curved surface the shape of which could be described analytically. It was found wanting when applied to an actual industrial pressing, the mapping procedure failed in severely deformed regions of the component which had also proved to be areas prone to wrinkling in the part.

It is recognized that the equal area hypothesis imposed in this work is likely to be too restrictive for many components. However, this condition can be relaxed and it is here that the experienced tool designer can use the technique in an interactive mode. The designer imposes alternative geometric rules which he deems are more suited to certain areas of the pressing, at the same time certain boundary conditions might be specified, i.e. certain sections of the boundary may be restricted from drawing-in as freely as other regions due to the use of draw beads and the like.

The method will not give rise to a unique solution to a problem, but its possibilities are worth pursuing, particularly when being manipulated by an expert tool designer. The execution time is likely to be minimal when compared with more rigorous analyses, such as finite element procedures. As yet this latter technique has been restricted to simple geometric shapes (e.g. axisymmetric components), and the process is modelled from the undeformed blank to the final deformed shape. The analytical procedures are not straight forward, furthermore the interfacial frictional conditions between tool and the workpiece and also certain boundary conditions are not known precisely. These parameters tend to be adjusted in an ad hoc manner until some acceptable solution is arrived at. These comments are not meant to minimize the worth of more involved analytical procedures, but rather to suggest there may be much to be gained by first attempting the less rigorous geometric modelling method.

PROPOSED AREAS OF FUTURE WORK

In light of the inadequacies of the modelling the following major areas of improvement should be studied in more detail.

(1) The assumption of constant area of a quadrilateral element is limited only to forming operations when no thinning occurs in the through thickness direction. When dealing with processes such as hydrostatic bulging of a sheet metal diaphragm, the area of an element changes at the pole. Consequently control

features should be added to the computer program, so that the designer may change the area of a quadrilaterial according to his own experience.

(2) The strategy used for locating the fourth node for any quadrilateral element would be physically correct if the diagonal happened to lie in a principal direction. This is unlikely and hence other strategies should be developed. Intuitively it seems that some method which minimizes the effective strain for the whole element would be appropriate.

(3) As indicated previously, the present mapping method can lead to large changes in the area of one half of a quadrilateral element and consequently large, but opposite changes, in the other half for compensation. This causes overlapping of material elements. Some relaxation procedure or smoothing techniques should be developed in addition to the alternative strategy proposed in (1).

(4) The resulting grid obtained by the transformation does not provide much information to the designer other than to delineate a possible boundary for the blank. Two further steps would be useful.

(a) Calculate for each node the principal strains and the principal directions imposed on the sheet in transforming from the plane to the curved surface and illustrate these by contours on a plot. The fundamental total large strain theories described in Chapter 3 permit these extensions.

(b) Obtain from the solution shown, say in Figure 5.9, the displacements of each node and use this to transform a regular array of square grids in the plane surface onto the curved surface. This transformation should closely follow the geometric rules for the original transformation of the hand-drawn grid and, with experience, one could interpret a picture of the deformed regular mesh plotted in a similar fashion to Figure 5.7. Such a diagram can readily be rotated and enlarged in a computer graphics system and examined for problem areas.

APPENDIX A

Four of the numerical methods described in Chapter 2 are employed below to solve the plane strain sheet drawing of a rigid non-hardening solid through a frictionless wedge shaped die. A detailed account of each technique is provided.

A.1 THE SLAB METHOD

A.1.1 Analysis

Setting up horizontal equilibrium of forces, see Figure A1.

$$(\sigma_x + d\sigma_x)\, 2(h + dh) + 2qdh - 2h\sigma_x = 0 \qquad (1)$$

neglecting infinitesimal higher order terms, (1) simplifies to

$$(\sigma_x + q)dh + hd\sigma_x = 0 \qquad (2)$$

Since $\sigma_y = -q$, the Tresca yield criterion becomes

$$|\sigma_x + q| = k \qquad (3)$$

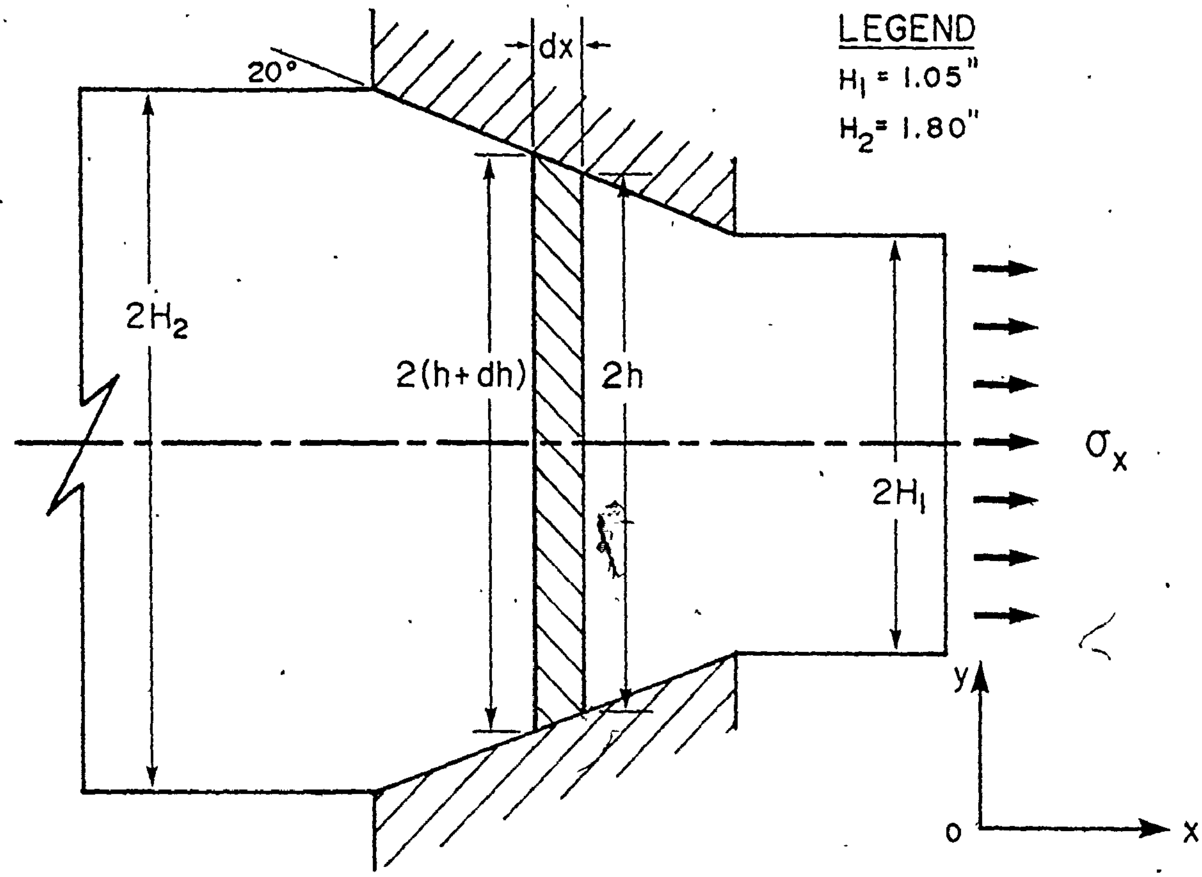

A1(a)

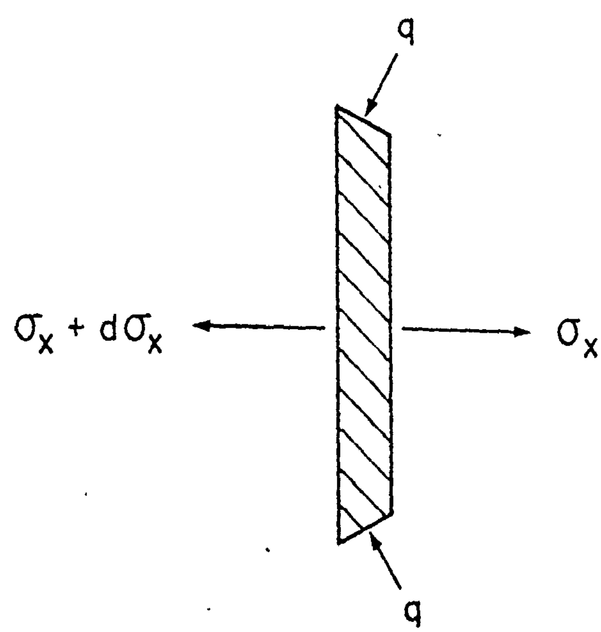

A1(b)

Figure A1 (a) Sheet drawing through a frictionless wedge-shaped die
(b) Free body diagram of a

By substitution equation (2) gives

$$kdh + hd\sigma_x = 0$$

or

$$\frac{dh}{h} = \frac{-d\sigma_x}{k} \tag{4}$$

By integration, gives

$$\ell n(ch) = \frac{-\sigma_x}{k} . \tag{5}$$

where c is a constant of integration. Solving for σ_x,

$$\sigma_x = -k \ \ell n(ch) \tag{6}$$

Consider boundary conditions:

At the entry: $h = H_2$ and $\sigma_x = 0$,

The constant of integration, c, is found to be

$$c = \frac{1}{H_2}$$

The axial stress distribution σ_x becomes

$$\sigma_x = -k\ell n(\frac{h}{H_2})$$

The drawing stress at the exit, when $h = H_1$, gives

$$\sigma_x = k\ln\left(\frac{H_2}{H_1}\right)$$

In the present example $H_1 = 1.05"$, $H_2 = 1.80"$. Therefore the required drawing stress is

$$\sigma_x = k\ln\left(\frac{1.80}{1.05}\right)$$

$$= 0.539\,k$$

A.2 THE UPPER BOUND SOLUTION

A.2.1 Analysis

Considering the geometry shown in Figure A2.

$$AB = \frac{H_2}{\sin 59^\circ} = 1.1666\ H_2$$

$$BC = \frac{AB}{\sin 70^\circ}\sin 71^\circ = \frac{H_2}{\sin 59^\circ}\,\frac{\sin 71^\circ}{\sin 70^\circ} = 1.1739\ H_2$$

From velocity diagram

$$V^*_{AB} = \frac{V_1}{\sin 39^\circ}\sin 20^\circ = 0.5435\ V_1$$

$$V^*_{BC} = \frac{V^*_{AB}}{\sin 50^\circ}\sin 59^\circ$$

$$= \frac{\sin 20°}{\sin 39°} * \frac{\sin 59°}{\sin 50°} V_1 = 0.6081\ V_1$$

volume flow rate: $V_1 H_2 = V_2 H_1$

The energy dissipated is:

$$\Delta\dot{\omega} = k(V^*_{AB} \cdot AB + V^*_{BC} \cdot BC)$$

rate of work done by the drawing stress, σ_x

$$\dot{w} = \sigma_x \cdot H_1 \cdot V_2$$

Equating the two work rate, yields

$$\sigma_x \cdot H_1 \cdot V_2 = k(V^*_{AB} \cdot AB + V^*_{BC} \cdot BC)$$

$$\sigma_x = \frac{k}{H_1 V_2} (V^*_{AB} \cdot AB + V^*_{BC} \cdot BC)$$

$$= \frac{k}{H_1 V_2} (0.5435 V_1 * 1.1666 H_2 + 0.6081 V_1 * 1.1739 H_2)$$

$$= 1.3479\ k$$

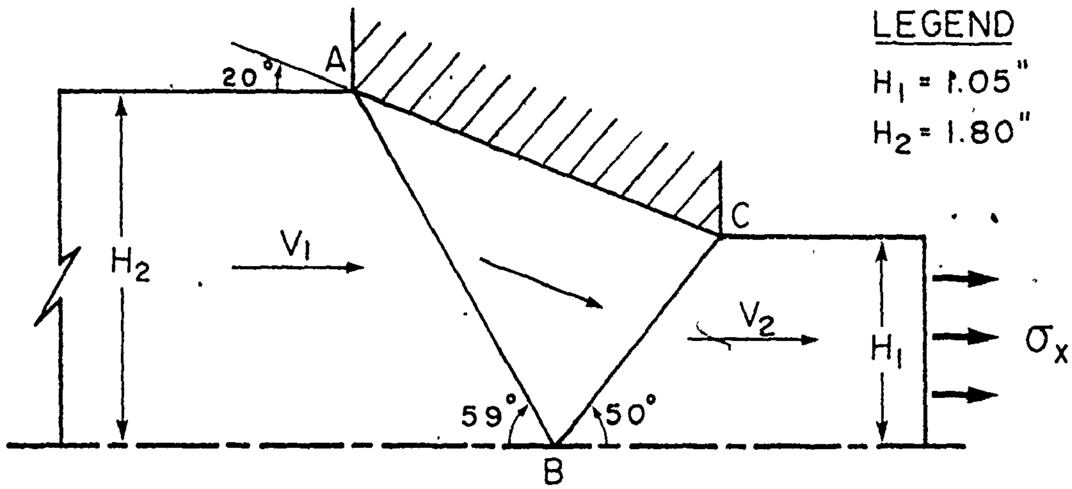

A2(a)

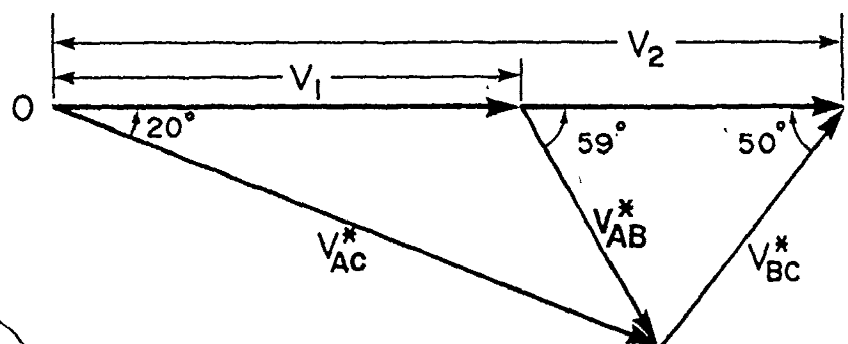

A2(b)

Figure A2 (a) An upper bound solution for sheet drawing
(b) Velocity diagram to (a)

A.3 THE LOWER BOUND SOLUTION

A.3.1 Analysis

Geometric consideration, see Figure A3.

$$P_1P_2 = \frac{ap_1}{\sin 39} \sin 20$$

$$= \frac{\sin 20}{\sin 39} k \text{ (since } ap_1 = k)$$

$$P_1P_3 = \frac{P_1P_2}{\sin 50} \sin 71$$

$$= \frac{\sin 20}{\sin 39} \cdot \frac{\sin 71}{\sin 50} k$$

$$= 0.6708 \text{ k}$$

or $$\sigma_x = 0.6708 \text{ k}$$

A.4 THE SLIP LINE FIELD TECHNIQUE

A.4.1 Analysis

The slip line field shown in Figure A4(a) is constructed and the die reduction ratio r is defined as,

$$r = \frac{\text{entry height - exit height}}{\text{entry height}}$$

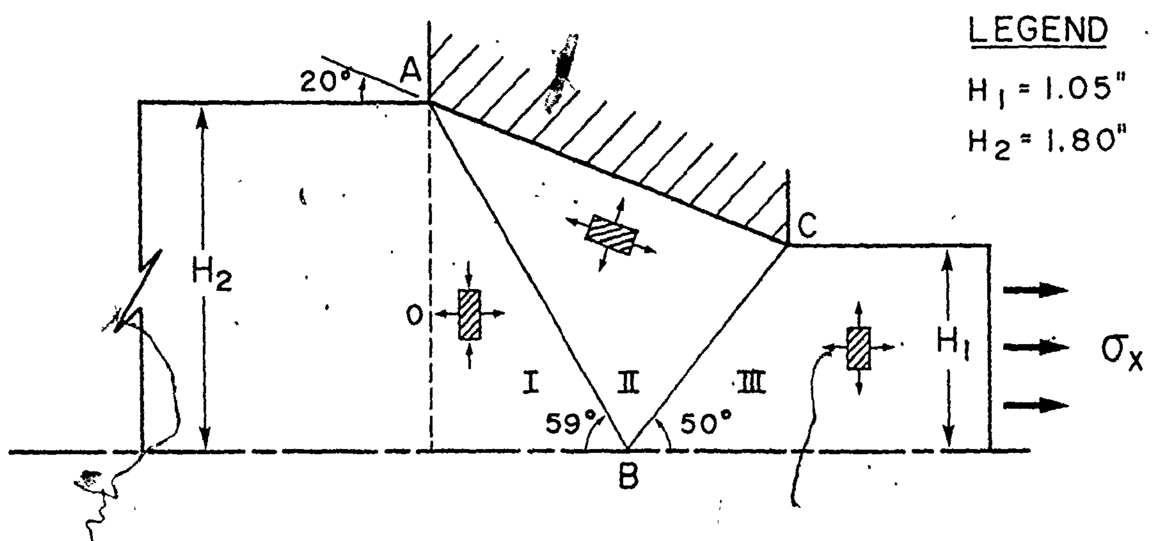

A3(a)

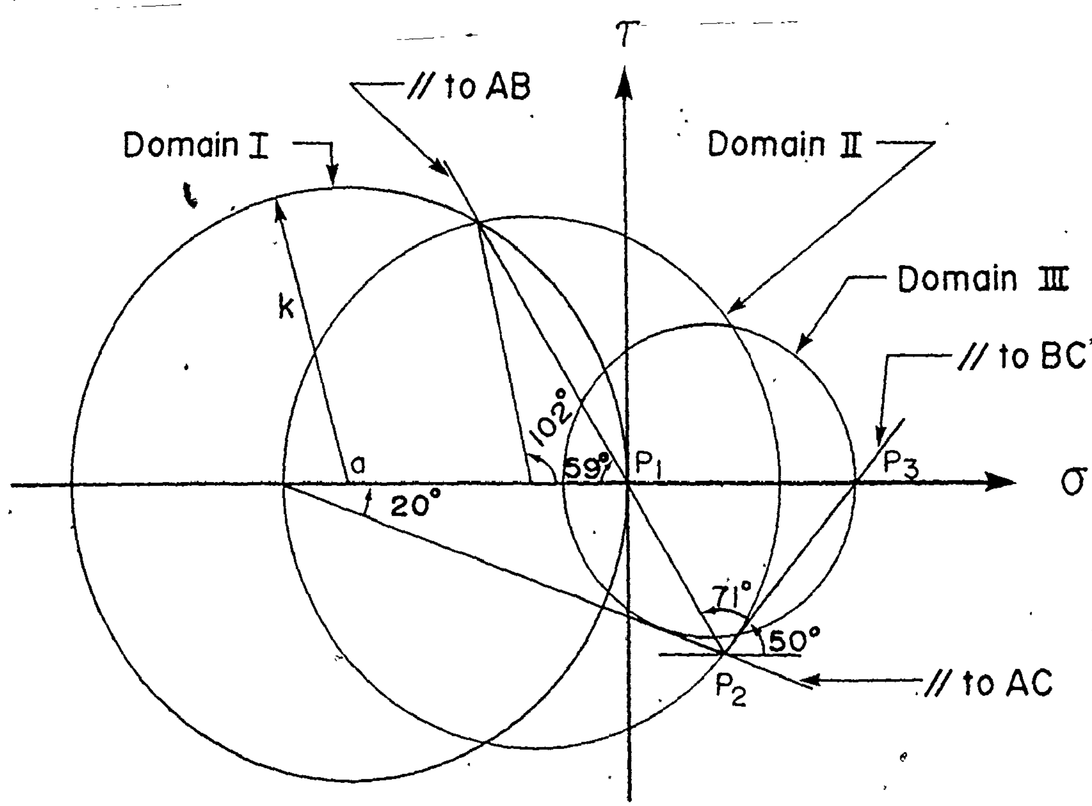

A3(b)

Figure A3 (a) A lower bound solution for sheet drawing through a frictionless wedge-shaped die
(b) Stress circles to (a)

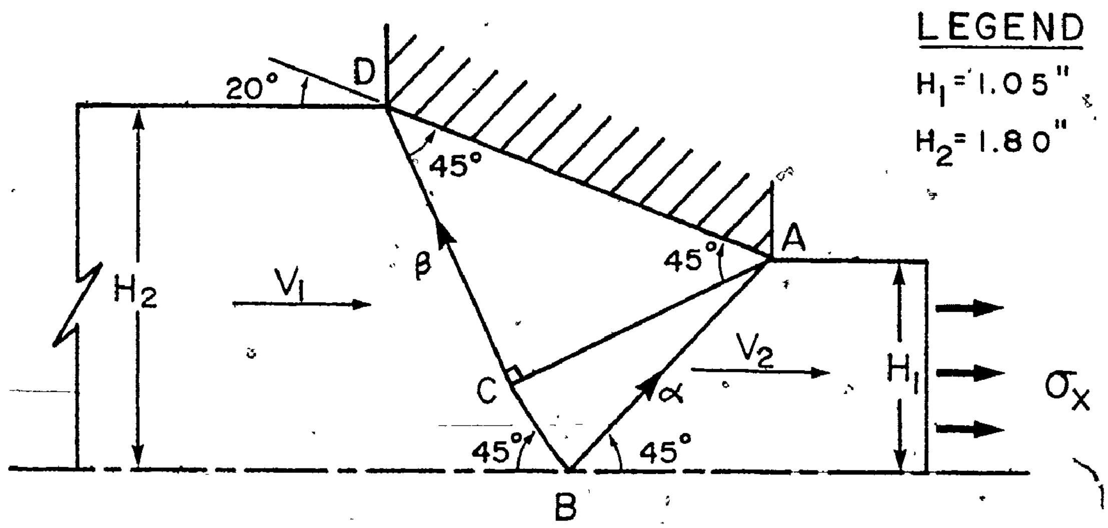

A4(a)

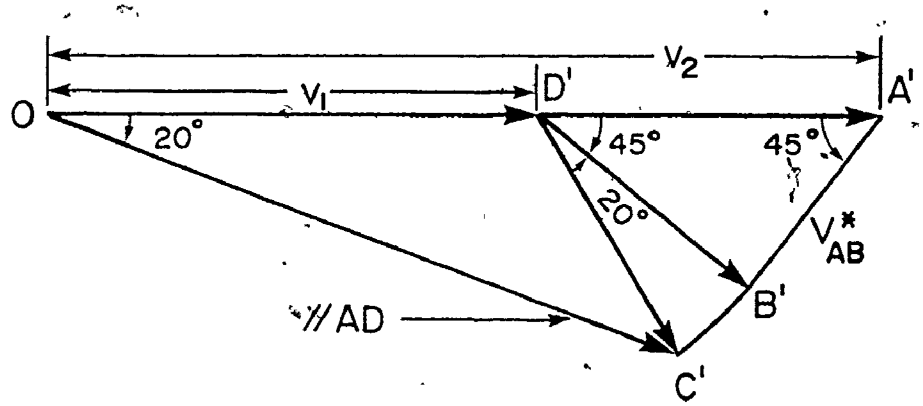

A4(b)

Figure A4 (a) A simple slip-line field solution for sheet drawing
(b) Hodograph to (a)

$$= \frac{H_2 - H_1}{H_1}$$

$$= \frac{(H_1 + AD\ \sin\alpha) - H_1}{H_1 + AD\ \sin\alpha}$$

$$= \frac{(H_1 + 2H_1\ \sin\alpha) - H_1}{H_1 + 2H_1\ \sin\alpha}$$

$$= \frac{2\sin\alpha}{1 + 2\sin\alpha}$$

It is easy to establish that AB is an α-line and BCD a β-line. Along AB the hydrostatic pressure, P_B, is compressive but not equal to k. From Figure A4(a).

$$\sigma_x = k - P_B$$

Applying the Hencky equation to β-line BCD

$$P_B - 2K\phi_B = P_C - 2K\phi_C$$

therefore $$P_C = P_B + 2K\alpha$$

The pressure on the die wall q is given by

$$q = P_C + K$$

$$= P_B + 2K\alpha + K$$

For equilibrium

$$q * (H_2 - H_1) = \sigma_x * H_1$$

Substituting $r = (H_2 - H_1)/H_2$, gives

$$\sigma_x = \frac{qr}{1-r}$$

Substituting for σ_x and q interms of P_B

$$(k - P_B)(1-r) = (P_B + 2K\alpha + K)r$$

or $$P_B = K(1-2r) - 2k\alpha r$$

Since $\sigma_x = K - P_B$

$$= 2Kr + 2k\alpha r$$

$$= 2Kr(1+\alpha)$$

Substituting $r = (2\sin\alpha)/(1+2\sin\alpha)$, the drawing stress is found to be

$$\sigma_x = 4k(1+\alpha)\frac{\sin\alpha}{(1+2\sin\alpha)}$$

Now $\alpha = 20^{o}$, yields

$$\sigma_x = 1.096.k$$

Final Remarks

The preceding example reinforces some of the statements made in Chapter 2. It is verified that in the absence of friction the Slab method provides the homogeneous work solution, and therefore does not account for redundant work. Friction could be incorporated into the analysis, but the present solution serves to emphasize the neglect of redundant work.

The results from the upper and lower bound methods straddle the Slip Line Field solution from above and below respectively. This is consistent with the underlying theory. No attempt has been made to optimize the results from the bounding techniques, i.e. to obtain the lowest upper bound and highest lower bound. However, the aim was to illustrate the solution procedures.

Note that the Slip Line solution does account for redundant work, as will be seen by comparing the result for the drawing stress with that obtained using the Slab method.

APPENDIX B

B.1 TRANSFORMATIONS OF FINITE STRAIN PARAMETERS

Consider the element OABC shown in Figure B.1(a) with a diagonal of length X_o and sides of length

$$OA = X_o \cos\theta$$
$$OC = X_o \sin\theta \tag{B.1}$$

the element is now deformed to element OA'B'C', by the strains E_{xx}, E_{yy}, E_{xy}, and E_{yx}. Point B is moved to B' and when referred to the x'- and y' axes the strain must give the same displacement.

Consider the component of displacement of B' along x'-axis. Equate this to the components of displacement of B' along x- and y-directions as shown in Figure B.1(b) where it is seen that

$$E_{x'x'} \cdot X_o = E_{xx} \cdot OA \cdot \cos\theta + E_{xy} \cdot OA \cdot \sin\theta + E_{yy} \cdot OC \cdot \sin\theta + E_{yx} \cdot OC \cdot \cos\theta$$

by substituting OA and OC from equations (B.1) into the above equation, gives

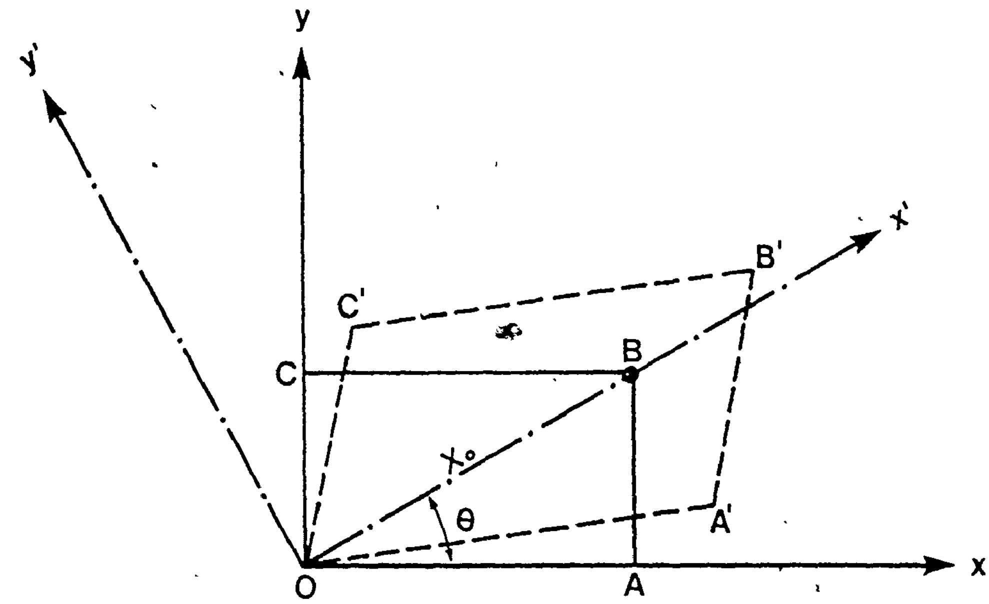

B.1(a)

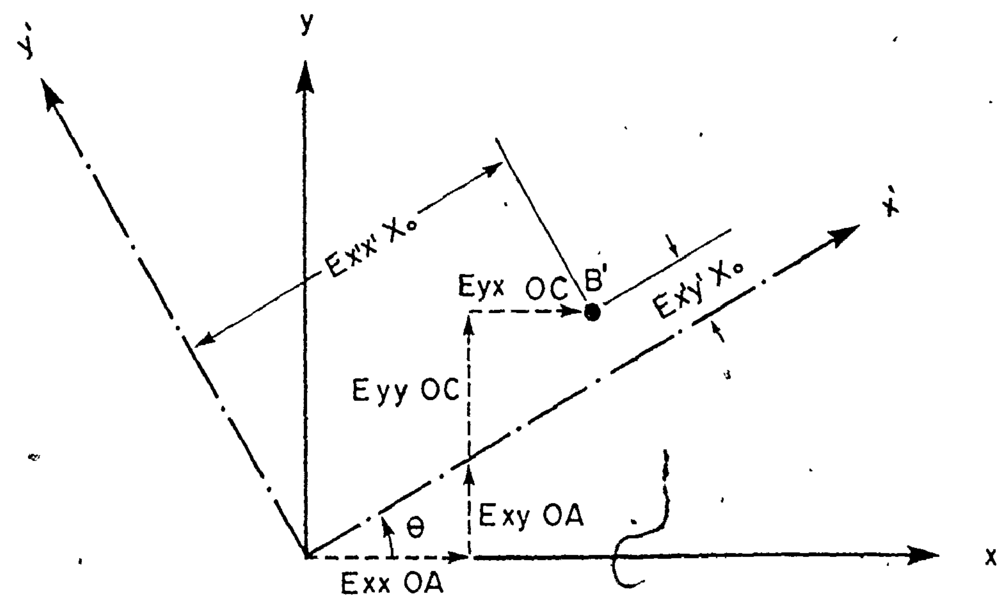

B.1(b)

Figure B1 Transformation of the finite strain parameters
(a) Relative deformation of an element
(b) Components of the displacement of point B with respect to the two orthogonal coordinate axes

$$E_{x'x'} \cdot X_o = E_{xx} \cdot X_o \cdot \cos^2\theta + E_{xy} \cdot X_o \cdot \cos\theta\sin\theta + E_{yy} \cdot X_o \cdot \sin^2\theta + E_{yx} \cdot X_o \cdot \cos\theta\sin\theta$$

$$E_{x'x'} = E_{xx}\frac{(1+\cos 2\theta)}{2} + E_{xy}\frac{\sin 2\theta}{2} + E_{yy}\frac{(1-\cos 2\theta)}{2} + E_{yx}\frac{\sin 2\theta}{2}$$

$$= \frac{E_{xx}+E_{yy}}{2} + \frac{E_{xx}-E_{yy}}{2}\cos 2\theta + \frac{E_{xy}+E_{yx}}{2}\sin 2\theta \qquad \text{(B.2)}$$

Now consider the component of displacement of B' along the y'-axis to that along the x- and y-directions, gives

$$E_{x'y'} \cdot X_o = -E_{xx} \cdot OA \cdot \sin\theta + E_{xy} \cdot OA \cdot \cos\theta + E_{yy} \cdot OC \cdot \cos\theta - E_{yx} \cdot OC \cdot \sin\theta$$

By substitutions, obtains

$$E_{x'y'} \cdot X_o = -E_{xx} \cdot X_o \cdot \cos\theta\sin\theta + E_{xy} \cdot X_o \cdot \cos^2\theta + E_{yy} \cdot X_o \cdot \cos\theta\sin\theta - E_{yx} \cdot X_o \cdot \sin^2\theta$$

$$E_{x'y'} = -E_{xx}\frac{\sin 2\theta}{2} + E_{yy}\frac{\sin 2\theta}{2} + E_{xy}\frac{(1+\cos 2\theta)}{2} - E_{yx}\frac{(1-\cos 2\theta)}{2}$$

$$= \frac{E_{xy}-E_{yx}}{2} + \frac{E_{xy}+E_{yx}}{2}\cos 2\theta - \frac{E_{xx}-E_{yy}}{2}\sin 2\theta \qquad \text{(B.3)}$$

If the shearing strains are defined so that $E_{xy} = E_{yx}$, the transformation equations becomes

$$E_{x'x'} = \frac{E_{xx} + E_{yy}}{2} + \frac{E_{xx} - E_{yy}}{2} \cos 2\theta + E_{xy} \cdot \sin 2\theta$$
$$E_{x'y'} = - \frac{E_{xx} - E_{yy}}{2} \sin 2\theta + E_{xy} \cdot \cos 2\theta \qquad \text{(B.4)}$$

B.2 MOHR'S CIRCLE OF FINITE STRAINS

A careful study of equations (B.4) shows that they represent a circle in space, which can be rewritten as

$$E_{x'x'} - \frac{E_{xx} + E_{yy}}{2} = \frac{E_{xx} - E_{yy}}{2} \cos 2\theta + E_{xy} \cdot \sin 2\theta$$
$$E_{x'y'} = - \frac{E_{xx} - E_{yy}}{2} \sin 2\theta + E_{xy} \cdot \cos 2\theta \qquad \text{(B.5)}$$

Then by squaring both of these equations, adding, and multiplying

$$(E_{x'x'} - \frac{E_{xx} + E_{yy}}{2})^2 + E^2_{x'y'} = (\frac{E_{xx} - E_{yy}}{2})^2 + E^2_{xy} \qquad \text{(B.6)}$$

equation (B.6) may be written in more compact form as

$$(E_{x'x'} - a)^2 + E^2_{x'y'} = b^2 \qquad \text{(B.7)}$$

where $a = \frac{E_{xx} + E_{yy}}{2}$ and

$b^2 = (\frac{E_{xx} - E_{yy}}{2})^2 + E^2_{x'y}$ are constants.

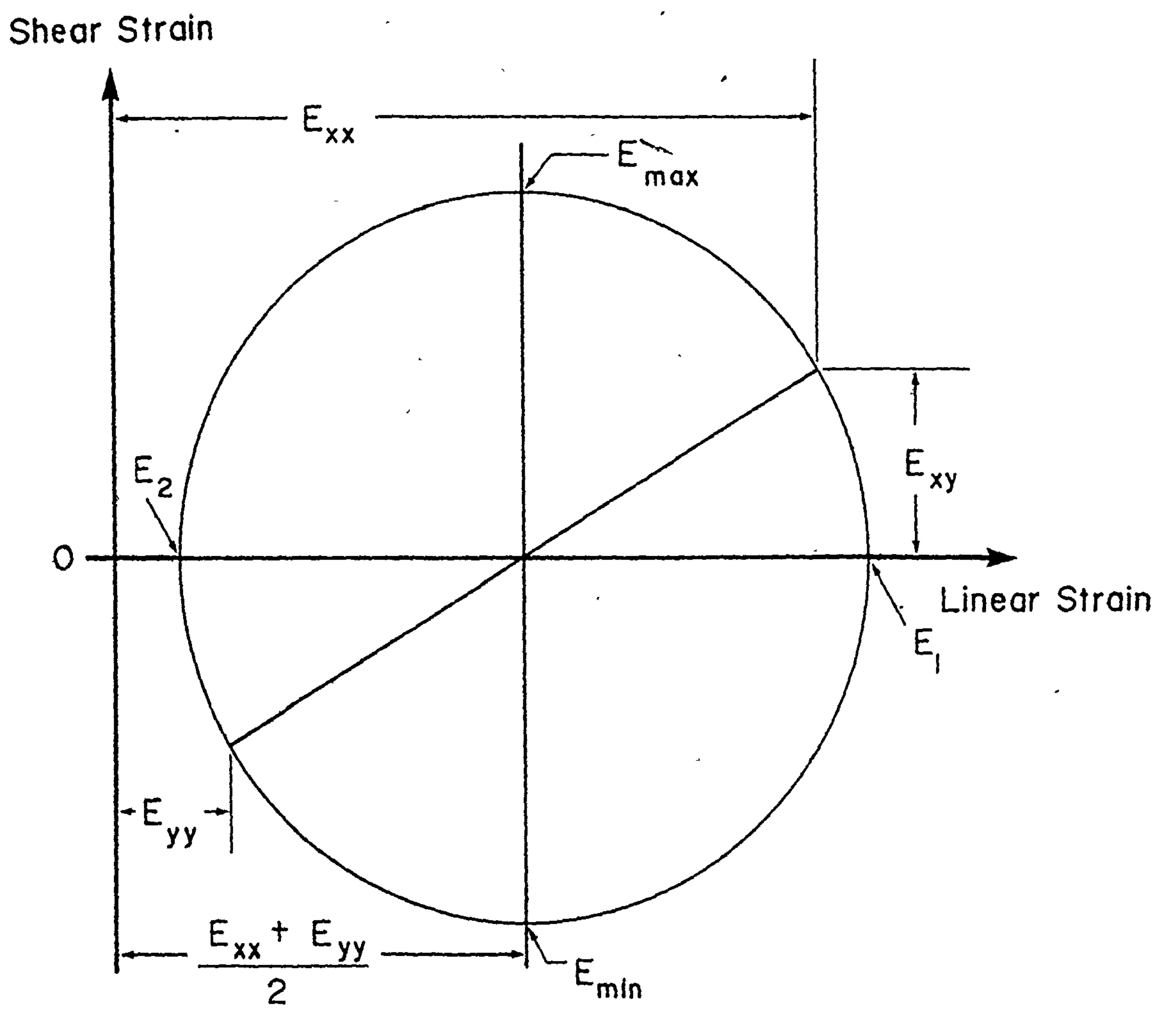

Figure B2 Mohr's circle of finite strains

This equation is the familiar expression for a circle of radius b with its centre at (a, 0). Hence a Mohr's circle can be constructed with the ordinate of a point on the circle as the shearing strain $E_{x'y'}$, and the abscissa is the linear strain $E_{x'x'}$. The circle so constructed is called a circle of strain or Mohr's circle of strain, as shown in Figure B.2.

APPENDIX C

C.1 FINITE STRAIN PARAMETERS OF A RECTANGULAR ELEMENT

The strain parameters are determined by the following definition (see Figure C.1).

$$
\begin{aligned}
E_{xx} &= (OA'' - OA)/OA \\
E_{xy} &= A'A''/OA \\
E_{yx} &= B'B''/OB \\
E_{yy} &= (OB'' - OB)/OB
\end{aligned}
\tag{C.1}
$$

The shear angle α is obtained from the condition that

$$V_A \cdot OB = U_B \cdot OA \tag{C.2}$$

hence $OB \cdot OA' \cdot \sin\alpha = OA \cdot OB' \cdot \sin[\theta' - (90 + \alpha)]$

Expanding gives

$$OB \cdot OA' \cdot \sin\alpha = OA \cdot OB' \cdot (-\sin\theta' \sin\alpha - \cos\theta' \cos\alpha)$$

$$
\begin{aligned}
OB \cdot OA' \cdot \sin\alpha = &- OA \cdot OB' \cdot \sin\theta' \sin\alpha \\
&- OA \cdot OB' \cdot \cos\theta' \cos\alpha
\end{aligned}
$$

$$(OB \cdot OA' + OA \cdot OB' \cdot \sin\theta')\sin\alpha = -OA \cdot OB' \cdot \cos\theta' \cos\alpha$$

$$\tan\alpha = \frac{-OA \cdot OB' \cdot \cos\theta'}{OA' \cdot OB + OA \cdot OB' \cdot \sin\theta'}$$

$$\alpha = \tan^{-1}\left(\frac{-OA \cdot OB' \cdot \cos\theta'}{OA' \cdot OB + OA \cdot OB' \cdot \sin\theta'}\right) \tag{C.3}$$

C.2 FINITE STRAIN PARAMETERS OF A PARALLELOGRAM

By virtually the same procedures as section C.1, the following quantities are determined.

$$\begin{aligned} E_{xx} &= (OA'' - OA)/OA \\ E_{xy} &= A'A''/OA \\ E_{yx} &= C'C''/OC \\ E_{yy} &= (OC'' - OC)/OC \end{aligned} \tag{C.4}$$

Assuming proportional deformation of point B, such that

$$\frac{CB}{OA} = \frac{C'B}{OA'}$$

the fictitious angle between sides OA' and OC' can easily be shown to be given by

$$\theta_1' = \tan^{-1}\left(\frac{OA \cdot OB' \cdot \cos\theta'}{OA \cdot OB' \cdot \cos\theta' - OA' \cdot OB \cdot \cos\theta}\right)$$

by employing equation (C.3) the shear angle can then be evaluated

$$\alpha = \tan^{-1}\left(\frac{-OA \cdot OC' \cdot \cos\theta_1'}{OA' \cdot OC + OA' \cdot OC' \cdot \sin\theta_1'} \right)$$

See also Figure C.2 to aid in interpreting the above notation.

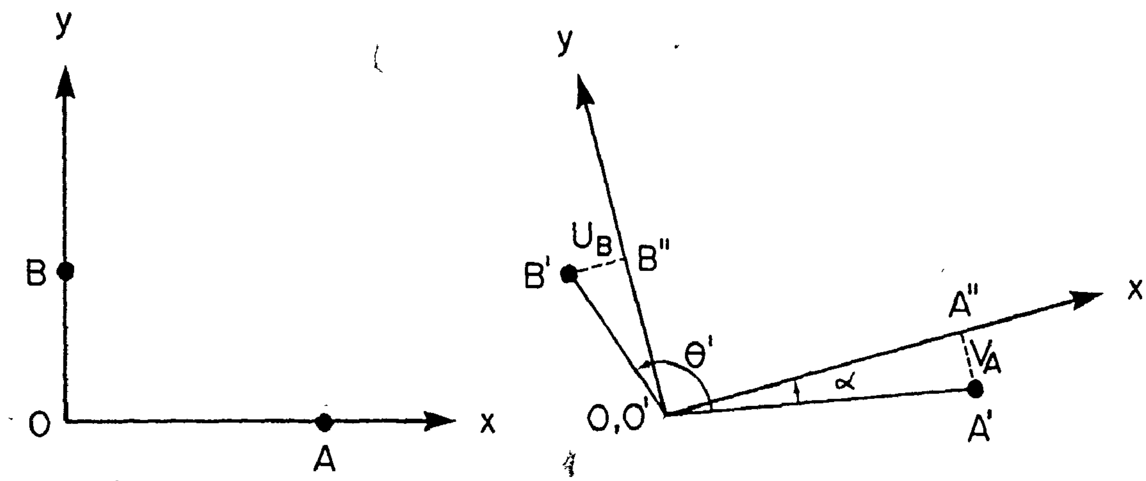

Figure C1 Diagrams showing the deformation of a rectangular element

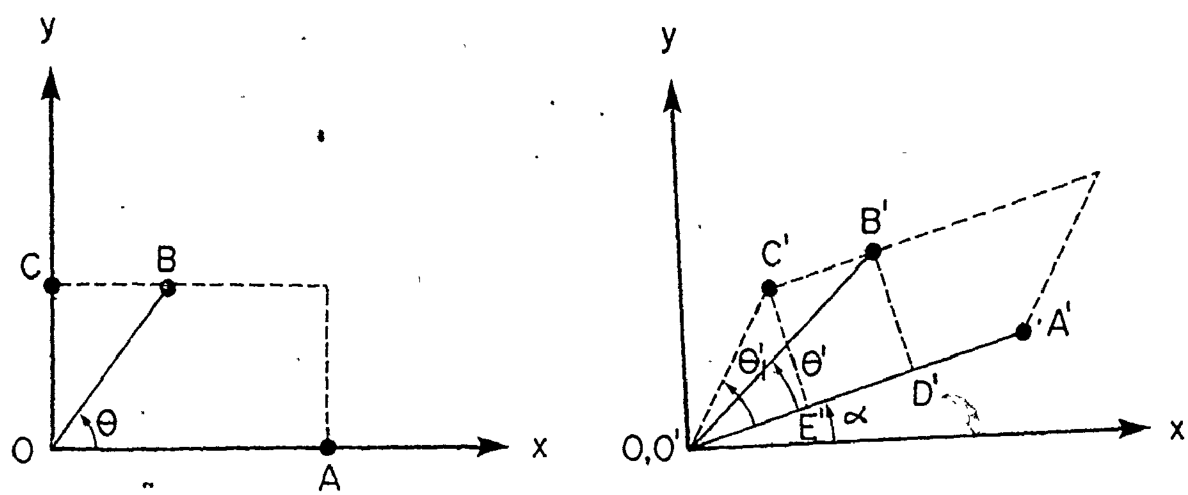

Figure C2 Diagrams illustrating the fictitious line length OC' and θ_1'

APPENDIX D

LIST OF SUBPROGRAMS

MAIN PROGRAM	- to generate and calculate the basic required storage for each principal variable.
SUBROUTINE GENMH	- to input sets of orthogonal coordinates, X, Y and Z of a formed part. To calculate element connectivity, nodal connectivity and to set up boundary conditions of a surface.
SUBROUTINE CHECK	- to check input data by plotting the geometry of a deformed part in 3D space using the Versatec 1200 A plotter.
SUBROUTINE SOLV	- to print results previously generated by GENMH, and to organize data for sequencial mapping
SUBROUTINE LOCAT	- to locate the coordinates of the fourth node of a quadrilateral in two dimensional space

SUBROUTINE CAL - an auxiliary subroutine for LOCAT, which computes the area, the sides and the angles of a triangle.

SUBROUTINE BLANK - to plot the developed blank using the Versatec plotter.

SUBROUTINE RES - to output the final X and Y coordinates of the transformed nodes of a blank.

SUBROUTINE FRAM - an auxiliary subroutine for plotting results.

SUBROUTINE DIAGEN - to transform the coordinates in a diagonal-wise fashion.

APPENDIX E

PROGRAM GLOSSARY

IE() - Element connectivity of triangular elements

- Storage required - 3*LE

- Function - to store node numbers of each triangular element in an anticlockwise direction

IR() - Element connectivity of quadrilateral elements

- Storage required - 2*LE

- Function - identical to array IE, but for a quadrilateral element

IW() - Nodal connectivity

- Storage required - 9*LW

- Functions - to store element numbers which are connected to a common node with a maximum of eight triangular elements, and to store code numbers for displacements u and v

I1, I2, I3, I4 - Node numbers of a quadrilateral

LE - Total number of triangular elements

LR - Total number of rectangular elements

LU, LV - Displacement codes for any nodes on a surface in X and Y directions, where:

0 - indicates nodes with zero component of displacement

1 - denotes free displacements

LW - Total number of nodes

NW1 - A constant calculated by 3*LW

NW2 - A constant of value 5*LW

NW3 - The sum of NW1 and NW2

RW() - Storage required - 8*LW + 3*LE

Functions - to store the coordinates X, Y, Z of each node in 3D space, the nodal coordinates X and Y in 2D space, and the resultant principal nodal strains ε_1 and ε_2.

RE() - Storage required - 2*LE

- Functions - to store principal element strain ε_1 and principal angle

REFERENCES

[1] "Engineering Plasticity: Theory of Metal Forming Processes", (Ed. by H. Lippmann), CISM Courses and Lectures No. 139, Springer-Verlag, vol. I & II (1977).

[2] Hoffman, O. and Sachs, G., "Theory of Plasticity", McGraw-Hill, New York (1953).

[3] Maclellan, G.D.S., J. Iron Steel Inst., 158, 347 (1948).

[4] Johnson, W., and Mellor, P.B., "Engineering Plasticity", Von Nostrand, London (1978).

[5] Backofen, W.A., "Deformation Processing", Addison-Wesley, Massachussetts, New York (1968).

[6] Avitzur, B., "Metal Forming: Processes and Analysis", McGraw-Hill, New York (1968).

[7] Johnson, W., Sowerby, R., and Haddow, J.B., "Plane Strain Slip Line Fields: Theory and Bibliography", Edward Arnold, London (1970).

[8] Zienkiewicz, O.C., "The Finite Element Method", McGraw-Hill, London (1977).

[9] Lee, C.H., and Kobayashi, S., J. Eng. for Ind., Trans. ASME, series B, 95, 865 (1973).

[10] Lee, E.H., Mallett, R.L., and Yang, W.H., Computer Methods Appl. Mechs. Eng., 10, 339 (1977).

[11] Sachs, G., Z. angew. Math. Methanik, 7, 235 (1927).

[12] Johnson, W., and Sowerby, R., Wire Ind., Feb., 137 and Mar., 249 (1969).

[13] Altan, T., and Nagpel, V., Int. Metals Reviews, 22, 322 (1977).

[14] Hill, R., Phil. Mag., 42, 868 (1951).

[15] Hill, R., "The Mathematical Theory of Plasticity", Oxford University Press (1956).

[16] Johnson, W., and Kudo, H., "The Mechanics of Metal Extrusion", Manchester University Press, England (1962).

[17] Avitzur, B., "Mètal Forming: The Application of Limit Anlaysis", Marcel Dekker, Inc., New York (1980).

[18] Collins, I.F., Proc. Royal Soc. Series A, 303, 317 (1968).

[19] Dewhurst, P., and Collins, I.F., Int. J. Num. Methods Eng., 7, 356 (1973).

[20] Christopherson, D.G., Palmer, W.B. and Oxley, P.L.B., Engineering, 186, 113 (1958).

[21] Johnson, W., and Sowerby, R., "Applications of Numerical Methods to Forming Processes", Ed. by H. Armen and R.F. Jones, published by ASME N.Y. (AMD-28), 1 (1978).

[22] John, J.E.A., "Gas Dynamics", Allen and Bacon, Inc., Toronto(1978).

[23] Szczepinski, W., "Introduction to the Mecahnics of Plastic Forming of Metals", Sijthoff & Noordhoff, Netherlands (1979).

[24] Yamada, Y., Yoshimura, N., and Sakurai, T., Int. J. Mech. Sci., 10, 343 (1968).

[25] Lee, C.H., and Kobayashi, S., J. Eng. for Ind., Trans. ASME, Series B, 95, 865 (1973).

[26] Tomita, Y., and Sowerby, R., Int. J. Mech. Sci., 20, 361 (1978).

[27] Yamada, Y., and Hirakawa, H., "Applications of Numerical Methods to Forming Processes", Ed. by H. Armen and R.F. Jones, published by ASME N.Y. (AMD-28), 27 (1978).

[28] LeRoy, G.H., Ph.D. Dissertation, McMaster University, Hamilton, Canada (1978).

[29] Danckert, J., and Wanheim, T., J. of Mech. Working Tech., 3, 5 (1979).

[30] Sklad, M.P., and Duncan, J.L., "A New Strain Parameter for Large Deformations", McMaster Engineering Report, October (1979).

[31] Sklad, M.P., and Duncan, J.L., "Determination of Total Strains", McMaster Engineering Report, October (1979).

[32] Sowerby, R., Chu, E., and Duncan, J.L., Unpublished work, (1981).

[33] Duncan, J.L., and Altan, T., Annals of CIRP, 29, 153 (1980).

[34] Keeler, S.P., S.A.E. paper No. 650635 (1965).

[35] Keeler, S.P., and Backofen, W.P., Trans. ASME, 56, 25 (1963).

[36] Havranek, J., Hobbs, R.M., and Brammer, I., Proc. 10th IDDRG Cong., Warwick, 121 (1978).